



Original Paper

Complex genesis of multiperiod fractures in the Middle Triassic Leikoupo Formation in the Pengzhou gas field, western Sichuan Basin, China



Xiao-Fei Hu ^{a, b}, Hu-Cheng Deng ^{a, b, *}, Jian-Hua He ^a, Zhong-Min Shen ^a, Xian-Feng Peng ^a

^a College of Energy, Chengdu University of Technology, Chengdu, Sichuan 610059, China

^b State Key Laboratory of Oil and Gas Reservoir Geology and Exploitation (Chengdu University of Technology), Chengdu, Sichuan 610059, China

ARTICLE INFO

Article history:

Received 28 October 2021

Received in revised form

18 September 2022

Accepted 2 October 2022

Available online 7 October 2022

Edited by Jie Hao and Jia-Jia Fei

Keywords:

Multiperiod fractures

Interaction relationships

Genesis mechanism

Gas migration

Leikoupo formation

Sichuan basin

ABSTRACT

The cumulative expression of multistage deformation is complex multiperiod fractures, which are commonly seen in tectonic zones. The Middle Triassic Leikoupo Formation in the western Sichuan Basin Depression, China, is a typical marine carbonate reservoir with natural fractures caused mainly by tectonic movements. According to outcrops, drill cores, image logging, and fluid inclusions, the fracture characteristics, types of natural fractures, and interactions of fractures are determined. In total, 419 natural fractures in 493.2 m of cores from 7 wells are investigated, which are mainly shear and tensile fractures with a small number of weathering generated fractures. Meanwhile, the results of the stable isotope analysis of $\delta^{13}\text{C}$ and $\delta^{18}\text{O}$, as well as the flow fluid inclusion data, reveal four tectonic periods of fractures with different occurrences. Based on the history of regional tectonic evolution, indicating one period of weathering fractures ascribable to stratal uplift and three periods of structural fractures related to the sequential tectonic movements of the Longmenshan fault belt. By analyzing the interaction relationships of fractures, three types of fracture interaction relationships are observed: cutting, restraining, and overlapping. The four stages fractures are chronologically assigned to (1) the early Indosinian N-S trending compression, (2) the late Indosinian NW-SE compression, (3) the middle Yanshanian NE-SE compression, and (4) the early Himalayan E-W compression. The influence of natural fractures on gas migration and well production in marine carbonates is discussed, and indicates that tectonic fractures could provide seepage channels for gas migration and accumulation from near or distant hydrocarbon source rocks into the Middle Triassic Leikoupo Formation. This study utilizes a pragmatic approach for understanding the fracture genesis mechanism in oil and gas field with multiperiod fractures.

© 2022 The Authors. Publishing services by Elsevier B.V. on behalf of KeAi Communications Co. Ltd. This is an open access article under the CC BY-NC-ND license (<http://creativecommons.org/licenses/by-nc-nd/4.0/>).

1. Introduction

The lineaments and internal characteristics of a single formation are an intuitive reflection of its spatial and temporal changes. The rapid changes, recurrence of the extents, and directions of these features indicate that deformation has occurred in more than one stage (Aghli et al., 2019; Scheiber and Viola, 2018). In the geological history experienced by strata, the old subsurface units usually undergo multistage deformation in which tectonic events are

superimposed on each other. The brittle deformation from tectonic movements is typically exhibited by multiscale and diverse types of faults and fracture networks (Li et al., 2021a; Li et al., 2018). Due to the potential high permeability (Bense et al., 2013; Caine et al., 1996; Huang et al., 2020) and the high erodibility of brittle faulted strata (Molnar et al., 2007), the existence of fractures can strongly affect hydrocarbon enrichment and reservoir properties. Geologists focus on characterizing stratum deformation features for correlation because they exhibit an intuitive response to earth motion. It has been demonstrated to be critical to understanding hydrocarbon transit and storage in pore network systems (Branellec et al., 2015; Kosari et al., 2017).

In sedimentary basins, fractured hydrocarbon reservoirs are

* Corresponding author. College of Energy, Chengdu University of Technology, Chengdu, Sichuan 610059, China.

E-mail address: denghucheng@cdu.cn (H.-C. Deng).

important regions to look for high-yield energy resources (Yang et al., 2011; Zhang and Yin, 2017). The key areas for the storage and transit of hydrocarbons are structural fractures. As a result, the key prerequisite for properly exploiting a fractured hydrocarbon resource is to understand the distribution and genesis of fractures. Indeed, fracture patterns may provide insightful information relating not only to the regional strain history but also to the process of stress genesis (Branellec et al., 2015; Song et al., 2020). At present, the practice of field production and research results have shown that it is difficult to precisely predict fractures with a single discipline or method (Deng et al., 2018). Geological investigations, experimental tests, and numerical simulation methods are utilized to study the genetic mechanisms and development stages of structural stages; these approaches include geological outcrop surveys, drill core observations (Li et al., 2021b), carbon and oxygen isotope analyses (Gonzalez and Lohmann, 1985; Keith and Weber, 1964; Talbot, 1990), fluid inclusion analyses (Bakker, 2003; Frezzotti et al., 2012; Roedder, 1990), and rock acoustic emission techniques (Hardy, 1972, 1981; Lockner, 1993), which are effective ways to explore structural fractures. However, fractures usually have the characteristics of multistage genesis, reactivation, and filling, and each method or technique has limitations or multiple solutions (Bodnar, 1990; Corfield, 1995; Guo et al., 2019; Ren and Lin, 2007). Therefore, a necessary step is to integrate multiple methods and parameters to investigate the fracture system to improve the efficiency of reservoir exploitation. Based on the progressive methods and information, several studies have successfully revealed complex deformation histories of strata by using kinematic analysis, modeling calculation and detailed geometric analysis (Croix et al., 2019; Fischer and Christensen, 2004; Homberg et al., 2010; Li et al., 2020; Lyu et al., 2017; Özkaya, 2019; Pang et al., 2017; Saintot et al., 2011; Wang et al., 2020; Zhang et al., 2020). Although some findings imply that using fracture examination as a method is difficult, it does provide valuable evidence that reveals previous strata deformation, stress levels, and tectonic movements (Aghli et al., 2020; Ahmadhadi et al., 2007; Croix et al., 2018; Deng et al., 2018; Weil and Yonkee, 2012).

The Sichuan Basin is one of the most hydrocarbon rich regions in China. The Middle Triassic Leikoupo Formation (247.2–242 Ma) is an assemblage of anhydrite-dominated evaporites and carbonates, and is an important target for marine carbonate gas exploration in the Sichuan Basin (Jiang et al., 2019; Li et al., 2012; Lin and Chen, 2008). During more than 40 years of petroleum resource exploration, two medium-sized reservoirs, the Moxi and Zhongba gas fields, have been found in the Middle Triassic Leikoupo Formation (Li et al., 2011; Liu et al., 2012; Zhu et al., 2011), and a number of gas-bearing structures have been discovered, e.g., Longnvi, Tongnan, Luoduxi, Guanyinchang, and Yuanba-Longgang (Jiang et al., 2019). Previous development and studies have found that one of the keys to exploring for resources in the Leikoupo Formation is the migration channels connecting hydrocarbon source rocks and reservoirs (Liu et al., 2011; Wang et al., 1998). Due to the complex tectonic geological conditions, especially reservoir genesis, intricate structural stress fields, and multiple periods of fractures sets, there are still many obstacles, such as natural gas enrichment regularity and fracture genesis. Since 2006, initial exploration wells, such as CK1, XS1, and PZ1, have made a major breakthrough in the Leikoupo Formation, generating industrial natural gas flow (Song et al., 2013), and it has been proven that natural gas reserves of the Chuanxi/Pengzhou gas field are $1140 \times 10^8 \text{ m}^3$ (Zhang et al., 2021). Previous studies show that the shoal dolomite reservoirs in the Leikoupo Formation are fracture-pore types of reservoirs that experienced multiple stages tectonic movements (Ding et al., 2018; Meng et al., 2015). He et al. (2019) show the detailed fracture characteristics, such as fracture attitude and density, in the Leikoupo Formation. Li

et al. (2016) present that multiple periods of tectonic movements allowed for the formation of micro-faults and fractures that are beneficial to the enrichment of hydrocarbons in the Leikoupo Formation. Zhang et al. (2022) analyze the lithologically-controlled fracture networks on gas migration and accumulation in the Leikoupo Formation. However, there is still a lack of insight studies on fractures, such as the characteristics of fractures corresponding to different periods of tectonic movement in the Leikoupo Formation, the development features of fractures in complex multistage tectonic superposition states, and their effects on oil and gas transport. Consequently, the Leikoupo Formation in the Sichuan Basin is a hydrocarbon rich formation worthy of further in-depth exploration.

In this study, we investigate the fracture characteristics in the Middle Triassic Leikoupo Formation in the western Sichuan Depression by utilizing outcrops, drill cores, thin sections, image logging, carbon and oxygen isotope analysis, and fluid inclusion tests. Then, we examine the genetic mechanism of multiperiod fractures and deduce the period of fracture genesis. Next, the crosscutting relationships between these fracture groups and their burial history are investigated. Finally, we develop a genetic model of multiperiod fractures in the Leikoupo Formation, which has undergone significant tectonic movement. Fractures and their impact on gas migration and production are also discussed. The interactive relationships between multistage fractures and development mechanisms are revealed in this paper, which could provide a geological foundation for exploring fractured marine carbonate reservoirs.

2. Geological setting

2.1. Location and structure

The Longmenshan fault belt is located between the Guankou fault and Pengxian fault in the western petroliferous Sichuan Basin Depression. It contains two integral secondary local structures, the Jinma-Yazihe and Shiyangchang tectonic units with trap areas of 162 km² and 28.9 km², respectively (Li et al., 2016). Since the Indosinian period, a series of tectonic evolutions was constrained by the Longmenshan fault belt (Chen et al., 2017; He et al., 2019), which remained at structural highs that contributed to gas accumulation. The Pengzhou gas field is one of the significant areas for hydrocarbon resource exploration in the south-central of the Longmenshan fault belt (Fig. 1) (Hu and Su, 2018). Petroleum exploration was initiated in the 1970s in this area, where the marine Leikoupo Formation contains enormous potential of natural gas resources.

2.2. Stratigraphic characteristics

The Leikoupo Formation is predominantly distributed in the west-central Sichuan Basin, which stretches to the southeast (Sichuan Provincial Bureau of Geology and Mineral Resources, 1991; Guo et al., 1996). The Leikoupo Formation lithologies are gray and/or brown primarily laminated aggregate dolomite and argillaceous dolomite with thin interlayers of limestone or gypsum. The Leikoupo Formation thickness is 0–1000 m (Fig. 2) and can be divided into 4 members, in which the thickness of the reservoir is around 100 m in the Lei-4 Member. The boundary between the Leikoupo Formation and the top of the Jialingjiang Formation is marked by green pisolites, with thickness of 0.5–3 m (He et al., 2019). Around the late Middle Triassic, the ancient land of Longmenshan was distributed like a string of beads in the northwestern Sichuan Basin, which intermittently separated the west Sichuan Depression and the Songpan oceanic trough in the north. During the deposition of the Leikoupo Formation, the paleogeography and

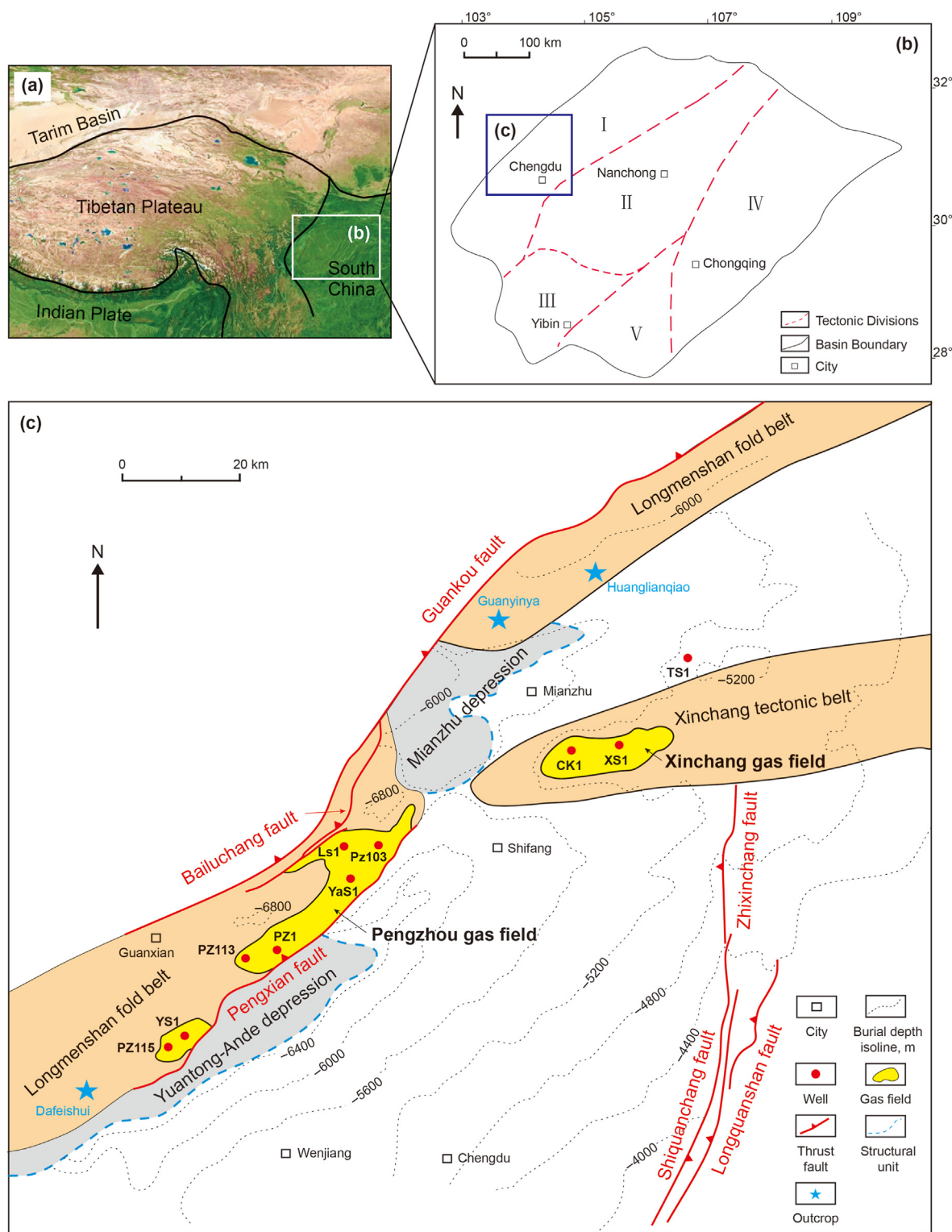


Fig. 1. (a) The tectonic units in the Central Asia area. (b) The tectonic units in the Sichuan Basin, China. I: Western Sichuan low-steep structural belt, II: Central Sichuan low-flat belt, III: Southwestern Sichuan low-steep structural belt, IV: Eastern Sichuan high-steep faulted fold belt, V: Southern Sichuan low-flat structural belt. (c) The location of the Pengzhou gas field and structural units on the top of the Leikoupo Formation in the Sichuan Basin (modified after (Li et al., 2016)).

sedimentary facies of the Sichuan Basin changed frequently, and the west Sichuan Depression gradually became a semiclosed epicontinental ocean basin (Feng et al., 1997; Liu and Tong, 2001). The top 4th member of the Leikoupo Formation was partially

eroded, with the thicknesses of 50–350 m. During this period, the Indosinian weathering crust formed karst reservoirs, which are unconformities that overlap with the Upper Triassic strata (Tang, 2013; Zhong et al., 2011).

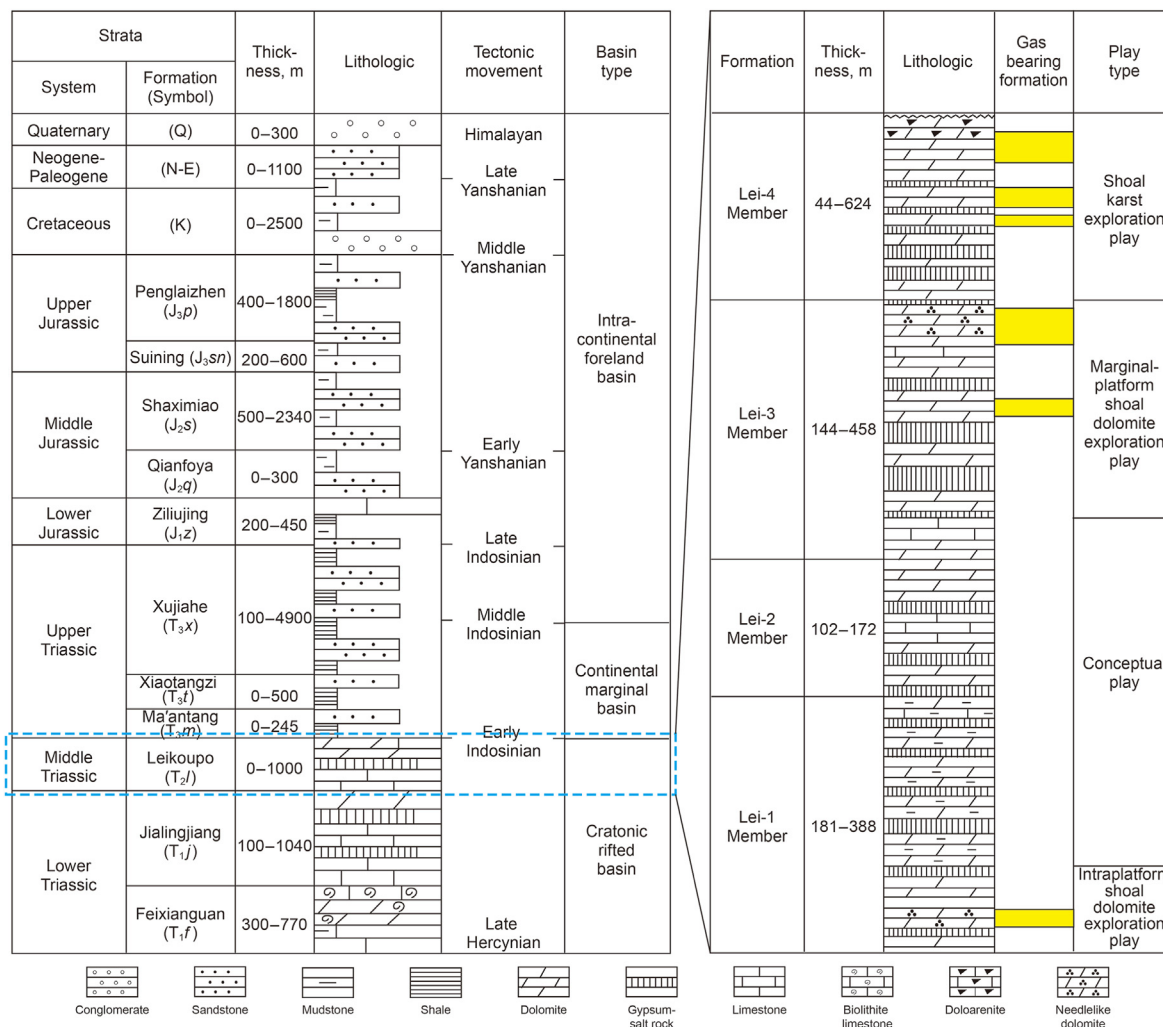


Fig. 2. Generalized stratigraphy and tectonic events of the Longmenshan orogenic zone (modified from He et al. (2019)).

2.3. Multiperiod tectonic characteristics

In the late Middle Triassic, the early Indosinian movement resulted in strata uplift and exposed the middle and upper Yangtze regions to denudation. During this period, the marine carbonate depositional environment in most regions ended and was transformed to lacustrine fluvial environment (Dong et al., 2011; Li et al., 2018). Around the time of the middle Indosinian movement, the foreland basin system began to develop, Longmenshan was uplifted and the Pengzhou area became a piedmont depression. The prototype faults of the western Sichuan Basin formed. During the late Indosinian movement, tectonic deformation of Longmenshan thrust belt continuously occurred. Low-angle thrusting appeared in the Guankou fault and Pengxian fault. At the same time, Jinma-Yazihe and Shiyangchang has developed structural anticlines. The Longmenshan region transitioned from a platform sedimentary environment to an orogenic environment during the Late Triassic. The fold and early thrust occurred that formed a north-east orientation tectonic zone (Gao et al., 2018; Hu and Su, 2018). In results, the early period weathering-related fractures and structural fractures are prone to form during these stage.

Within the period of the Yanshanian movement, the Longmenshan fold belt was strongly compressed; e.g., multiple low-angle thrust wedges developed in the hanging wall of the

Guankou fault, and the Pengxian fault continued to be active and evolved the slip deformation along the Cambrian mudstone surface, as shown in Fig. 3 (Wen et al., 2013). The Leikoupo Formation continues to experience another stage of fracture development during this time when considerable deformation moves into the basin.

Since the Himalayan movement stage, the Guankou fault and the Pengxian fault have intensely thrust to the surface under the

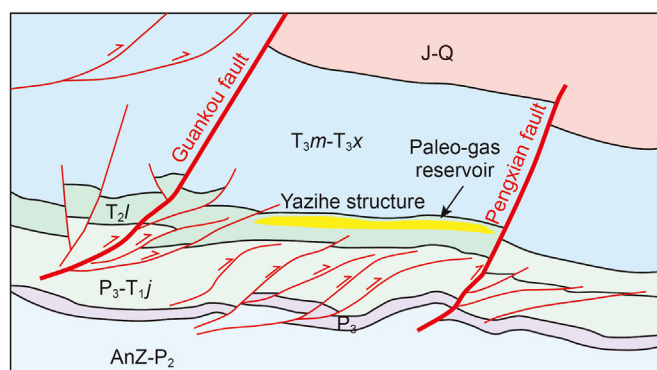


Fig. 3. Tectonic evolution of the Longmenshan piedmont tectonic belt (modified from Li et al. (2016)). From Late Yanshanian to Himalayan period.

control of the regional compressive and torsional stress fields (Shi et al., 2010; Xiong et al., 2020). In the Leikoupo formation, the latest structural-related fractures were developed during this stage. In general, the Jinma-Yazihe and Shiyangchang tectonic belts began in the late period of the Indosinian movement, continued to develop during the Yanshanian movement stage, and reached their final forms in the period of the Himalayan movement. As a result, the Leikoupo Formation experienced multiperiod structural movements that formed complex multiperiod fractures in the Pengzhou gas field.

3. Methods

Natural fractures in the Leikoupo Formation were described by visual inspections from outcrops along the Longmenshan fault belt and drill cores in the Pengzhou gas field. The core samples were taken from 7 wells in the Pengzhou gas field. A total of 493.2 m of cores from the 7 wells are investigated, and 419 natural fractures were identified. Observations works were concentrated on fracture characteristics, including fracture amount, fracture dip, fracture fills, fracture cutting relationships, etc.

Thin sections. In total, 125 thin sections of the Leikoupo Formation from the 7 wells were utilized to detail the microfracture characteristics using optical microscopy.

Stable carbon and oxygen isotope analysis. In this study, a total of 24 core fracture-fill samples from 7 wells were utilized for test. The fracture fill sample reacted with 100% orthophosphoric acid at a constant temperature to produce carbon dioxide and water. The collected carbon dioxide was purified, and then its $\delta^{13}\text{C}$ and $\delta^{18}\text{O}$ isotopic composition was determined by the gas isotope mass spectrometer. It is noted that the isotopic analysis follows the Chinese oil and gas industry standards of the Analysis Method for Carbon and Oxygen Isotopes in Organic Matter and Carbonate (SY/T 5238–2019) (CNEA, 2019). The experimental apparatus is the Delta V isotope ratio mass spectrometer (IRMS) from the State Key Laboratory of Oil and Gas Reservoir Geology and Exploitation in Chengdu, China. The experimental standard sample is the Chinese national standard sample (GBW04405). External precision for both $\delta^{13}\text{C}$ and $\delta^{18}\text{O}$ measurements is better than $\pm 0.2\%$ and $\pm 0.3\%$, respectively. The C and O isotopic compositions are reported in standard δ -notation relative to VPDB.

Fluid inclusion analysis. Fluid inclusions of fracture fills are those trapped in small pits in the mineral lattice during the crystallization period of minerals. Based on the evolution mechanism by which fluid inclusions are shaped synchronously with fracture fillings, fracture fill inclusions analysis was utilized to confirm the fracture period by measuring the temperature (Burruss et al., 1983; Li et al., 2019; Mourgues et al., 2012). Based on the China oil and gas industry standards of Micro Temperature Measurement Methods of Fluid Inclusion in Sedimentary Basins (SY/T6010-2011), a Renishaw inVia laser confocal microscopic Raman spectrometer and a Linkam THMS600 heating stage were used to analyze fluid inclusions. A total of 64 fluid inclusions from 25 calcite samples were tested. The fluid inclusions were heated using the heating stage. When a certain temperature was reached, the gas-liquid inclusions formed a single phase. This instantaneous temperature is the homogenization temperature of the fluid inclusion. Before the average temperature can be determined, the homogenization temperatures (Th) of each inclusion must be tested three times, with each Th having an absolute deviation of no more than 2 °C, to assure the reliability of test results.

4. Results

4.1. Petrologic characteristics

4.1.1. Fracture characterization

According to investigations of outcrops, natural fractures are well developed in the Leikoupo Formation, as shown in Fig. 4. As shown in Fig. 4a, based on the cutting relationships, the three groups of shear fractures can be divided into three stages: 1st, the seven fractures with average trends of SE ($130^\circ \pm 10^\circ$) \angle 85° filled by calcite. These fractures are mainly high-angle or vertical fractures with opening width from 0.5 to 5.0 mm; 2nd, a total of 10 fractures average trending of SE ($130^\circ \pm 10^\circ$) \angle 47° partly filled by calcite with opening width from 0.2 to 2.0 mm; 3rd, five fractures with average trends of NW ($270^\circ \pm 5^\circ$) \angle 55° with a significant longitudinal penetration that are partly filled by calcite with opening width from 0.2 to 1.2 mm. Fig. 4b presents the two sets of conjugate shear fractures. One group contains 10 fractures with average trending of SSW ($210^\circ \pm 10^\circ$) \angle 65° . And another 12 fractures with average E-W ($95^\circ \pm 10^\circ$) \angle 42° trending in dolomite. Fig. 4c shows gray-white granular dolomite of the Leikoupo Formation, in which two sets of shear fractures form a 13 fractures trending NEE ($75^\circ \pm 10^\circ$) \angle 36° and another 13 fractures trending SE ($140^\circ \pm 10^\circ$) \angle 58° , respectively. As shown in Fig. 4d, conjugate shear fractures observed with trends of SE ($140^\circ \pm 20^\circ$) \angle 12° and NEE ($265^\circ \pm 5^\circ$) \angle 20° in the gray-white granular dolomite partly filled by calcite and quartz. And another group of high-angle tensile fractures with trends of W-E ($75^\circ \pm 10^\circ$) \angle 75° are filled by calcite.

Based on the analysis of the composition and interaction relationships of fractures, three or four periods of fractures are identified (Fig. 5). In Fig. 5a–c, there are mainly high-angle or vertical fractures that are filled with carbonate, in which the fracture planes are relatively smooth. In these multiperiod fractures, one set is distributed in dense and uniform patterns of small scale, forming a conductively fractured network with no obvious directionality, which is filled by argillaceous and calcite (Fig. 5d and e). As for Fig. 5h–k, these fractures are the most unfilled, as shown in high-angle and low-angle views. Fig. 5l–m show the filled tensile fracture. Tensile fractures typically have an asymmetrical curve with an uneven distribution of seam width, and a limited extension. The thin section observation shows that there are at least three periods of fractures that interact with each other that are filled or unfilled, as presented in Fig. 5o–q.

4.1.2. Types of fractures

Fig. 6 demonstrates that tectonic fractures, namely shear fractures and tensile fractures accounting for 43.2% and 36.5%, respectively, are the major fracture types in the Leikoupo Formation, while weathering fractures account for 20.3%. On the other hand, as depicted in Fig. 7, the fractures are mainly net fractures, vertical fractures, and high-angle fractures. The vertical and high-angle fractures can extend 1.5 m with an openings of 0.1–0.5 cm. In addition, there are different filling degrees in various fractures. The net fractures, horizontal fractures, low-angle fractures, and high-angle fractures are mainly filled with carbonates and gypsums. However, the vertical fractures are mostly unfilled with smooth fracture surfaces and scratches, accounting for 20% of all fractures. In summary, based on the fill features and interaction relationships observed under the microscope, multiperiod fractures are easily discerned, in which the early period fractures are filled or partly filled while the late period fractures are mostly unfilled.

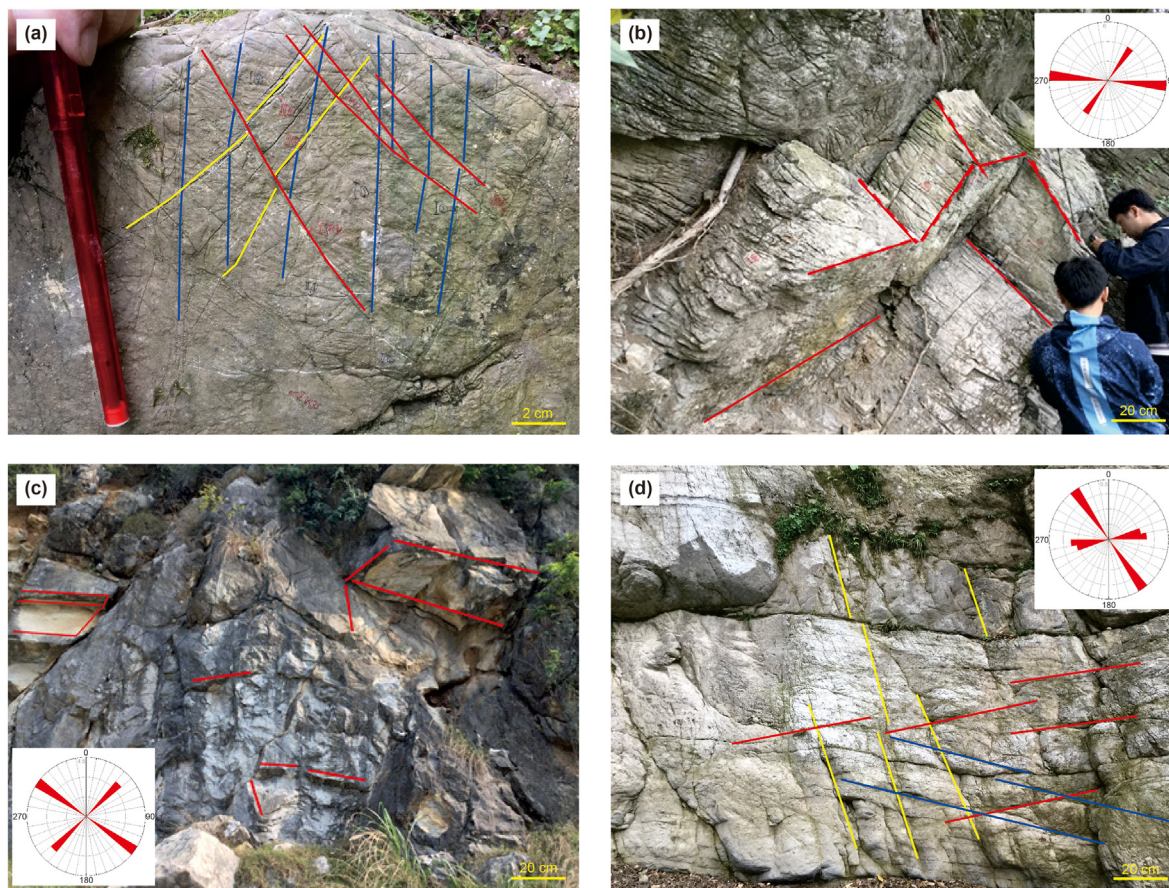


Fig. 4. Fracture characteristics of the Leikoupo Formation outcrops. (a) Three sets of interacting fractures, Dafeishui profile, Dayi county. (b) Conjugate shear fractures, Guanyinya profile, Mianzhu city. (c) Conjugate shear fractures, Huanglianqiao profile, Jiangyou city. (d) Three sets of interacting fractures, Dafeishui profile, Dayi county.

4.2. Geochemical characteristics

4.2.1. Carbon and oxygen stable isotopes

The carbon and oxygen isotopic compositions of calcite fracture fills can be used to differentiate between fracture stages and their diagenetic environments (Zhang et al., 2017). Any observed differences in data groups or calculated formation temperatures are most likely indicative of fracture formation stages (Amiri et al., 2015; Freund et al., 2013). The paleo-salinity can be inferred from the Z value calculated according to the formula proposed by Keith and Weber (1964). In this study, a total of 24 table isotopic test points are utilized for stable carbon and oxygen isotope analysis. Results show that the Z value of C–O stable isotopic ranges from 122.2 to 131.8, indicating a marine deposited environment.

The $\delta^{13}\text{C}$ values of Leikoupo Formation fracture fills range from -0.6‰ to 2.7‰ , with an average of 1.0‰ , and $\delta^{18}\text{O}$ ranges from -8.6‰ to -1.6‰ , averaging -5.3‰ , as presented in Fig. 8. Compared with the standard sample, the standard deviations of carbon and oxygen isotopes are both 0.1‰ . According to previous studies, the majority of modern marine inorganic carbonate worldwide have $\delta^{13}\text{C}$ and $\delta^{18}\text{O}$ values close to 0‰ and 0‰ , respectively, in the PDB standard (Faure, 1977; Veizer and Demovic, 1974). The variation of $\delta^{13}\text{C}$ and $\delta^{18}\text{O}$ values of the fracture-filled calcite range is larger than that of the enclosing carbonate. Note that the unfilled fractures, fractures filled with argillaceous materials or gypsum yield very little carbonate for isotopic analysis, and the relevant results for these fractures are not presented.

4.2.2. Fluid inclusions

Fluid inclusions are the solutions captured within mineral crystals during crystal growth, and inclusions are closed systems maintaining phase boundaries with the main mineral (Levine et al., 1991; Roedder, 1984). The fluid inclusions in the fracture fills represent sample of the original fluid from when the fracture developed; studying fluid inclusions is an effective method to investigate the genesis period of the fracture (Kelly et al., 2000). The tested fluid inclusions are secondary inclusions that persist in the fracture-filled dolomite and calcite minerals. Two-phase inclusions have diameters ranging from 2.1 to $15.6\ \mu\text{m}$ with vapor phase ratios between 7% and 25% (Table 1 in Appendix A. Supplementary material). It is worth noted that, carbonate mineral fluid inclusions are prone to post-trap volumetric re-equilibration, causing their Th to increase and approach the maximum temperature of the formation. Post-trapping changes in carbonated fluid inclusions are common, such as necking down, stretching, leakage, etc., which can disperse the Th distribution (Barker and Goldstein, 1990; Tobin and Claxton, 2000). In the field of fluid inclusions application, the relative study has emerged as a hot topic (Bourdet et al., 2010; Pironon and Bourdet, 2008). In this work, the test process is carried out in strict accordance with national standards in order to make the test results reliable, as mentioned above. This result excludes fluid inclusions, for example, that are too large or irregularly shaped. The temperature of each point is obtained and the measurement is repeated once more. The selected inclusions homogeneous temperature data are grouped and counted according to the



temperature range. These fluid inclusions in fracture fills present homogenization temperatures mainly ranging from 50 to 230 °C (Fig. 9). The analytical results show three major peaks of homogenization temperatures, namely 50–70 °C, 90–110 °C, and 170–190 °C, corresponding to (I) early period fractures, (II) secondary period fractures and (III) relatively late period fractures, which demonstrate that the Leikoupo Formation experienced at least three sequential periods of tectonic movement in the Pengzhou gas field.

5. Discussion

5.1. Interaction relationships of fractures

The Formation MicroImager (FMI) technique is widely utilized to investigate formation fractures, including natural fractures (opened and sealed) and drilling-induced fractures. Opened natural fractures are mostly filled by mud filtrate or low-resistance minerals that present black sinusoidal profiles on FMI images. Sealed natural fractures, generally filled by high resistance minerals, e.g., calcite, are formed by pressure solution, display a bright sinusoidal color curve on FMI images (Deng et al., 2018; Yang et al., 2014). Structural fractures are classified into three groups based on the sequence of fracture fillings, mineral components, fracture intercutting relationships, and the incidence of fractures recognized by FMI images (Yue et al., 2018). Through the FMI imaging and calibration of core observation, the three stages are substantially congruent with the results of the outcrop. Results show that the structural fractures can be grouped into three sets (Fig. 10). Fractures trending NW ($345^\circ \pm 5^\circ$) and W-E ($275^\circ \pm 5^\circ$) are “X”-shaped conjugate shear fractures belonging to the second period (Fig. 10b). Fractures trending NE ($35^\circ \pm 5^\circ$) and W-E ($275^\circ \pm 5^\circ$) are “X”-shaped conjugate shear fractures, which are relatively less developed, belonging to the third period. And fracture trending NE ($55^\circ \pm 5^\circ$) and SE ($125^\circ \pm 5^\circ$) are the most frequently found and are also “X”-shaped conjugate shear fractures that indicate the tectonic movement during the fourth period.

The characteristics of fractures in Leikoupo Formation show that the multiperiod fractures interact with and impact each other. The interaction relationships can be analyzed from their crosscutting relationships, fills, fracture distributions, etc. As aforementioned in Fig. 4, three sets of shear fractures, fully or partly filled, show that the area has experienced at least three periods of tectonic movements since the Leikoupo Formation was deposited. The early period fractures are mainly filled by the calcite; the middle period fractures are usually filled or half-filled by carbonates, and the later period fractures are mostly unfilled. Based on the results of thin section observations, three types of fracture interaction relationships are summarized for Leikoupo Formation (Fig. 11). In type I or cutting relationships, the main characteristic is that the late unfilled fractures cut the early filled fractures, causing dislocation of the early filled fractures, as shown in Fig. 11 (a–c). In type II or restraining relationships, the early fractures restrain the further extension or expansion of the late fractures; that is, the late fractures are terminated by the early fracture surfaces. Both early and late fractures can be filled or unfilled (Fig. 11 d–f). In type III or overlapping relationship, multiperiod fractures overlap or cross

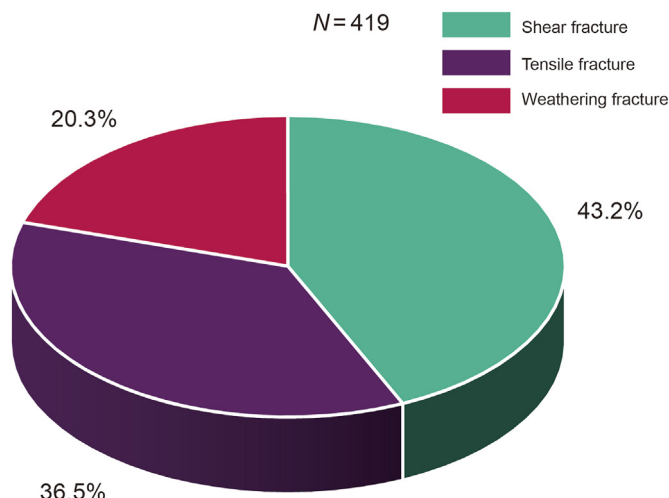


Fig. 6. Percentages of different genetic types of fractures in the Leikoupo Formation.

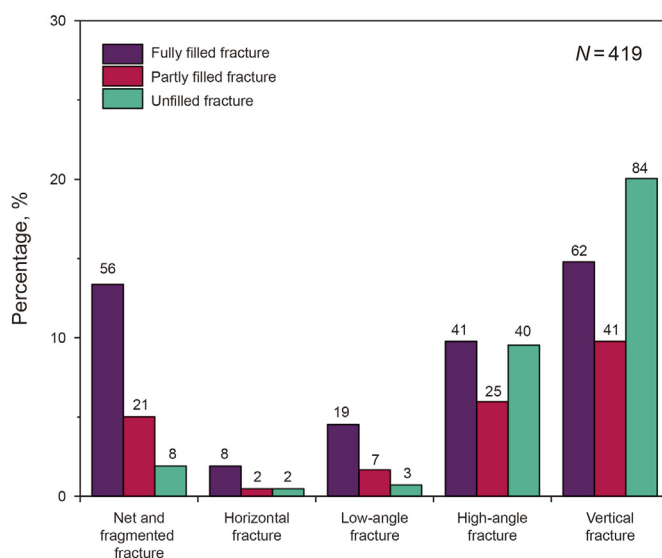


Fig. 7. Filling degrees of the different types of fracture in the Leikoupo Formation.

each other at a small angle (Fig. 11 g–i). The overlapping fractures are beneficial for the reservoir properties and the hydrocarbon transportation. Based on various types of fracture interaction relationships, it can be used as an effective tool to distinguish the formation sequence of fractures.

5.2. Fracture formation sequence

Based on the stable isotope analysis, the $\delta^{18}\text{O}$ of all samples is negative value with fairly most of positive $\delta^{13}\text{C}$ value. These results and fracture interaction relationship suggest that calcite fillings are precipitated at the same time as fracture develop. The $\delta^{18}\text{O}$ value has a negative trend, revealing that the characteristics of multiple

Fig. 5. Characteristics of multiperiod fractures from observations of drill cores and thin section from the Leikoupo Formation. (a) High-angle fractures, filled by gypsum, the fracture linear density is 0.66/m, LS1. (b) Three periods of high-angle fractures filled by gypsum, LS1. (c) Three periods of high-angle fractures filled with gypsum, LS1. (d) Weathering fractures, filled by argillaceous material, linear density 1.56/m, XS1. (e) Weathering fractures, filled by argillaceous material, linear density 3.05/m, PZ1. (f) Tectonic fracture fragments, XS1. (g) Tectonic fracture fragments, PZ1. (h) High-angle tectonic deformation fracture, unfilled, XS1. (i) High-angle tectonic deformation fracture, unfilled, linear density 0.67/m, YS1. (j) Low-angle shear fractures, half-filled by calcite, LS1. (k) Low-angle shear fractures, unfilled, YS1. (l) and (m) vertical tensile fractures, filled by gypsum, LS1. (n) Tensile fracture, filled by dolomite, XS1. (o) Four periods of fractures, where I and II are filled by calcite and III and IV are unfilled, LS1. (p) Three periods of fractures, where I and II are filled by calcite, LS1. (q) Three periods of fractures, where I and II are filled by calcite, LS1.

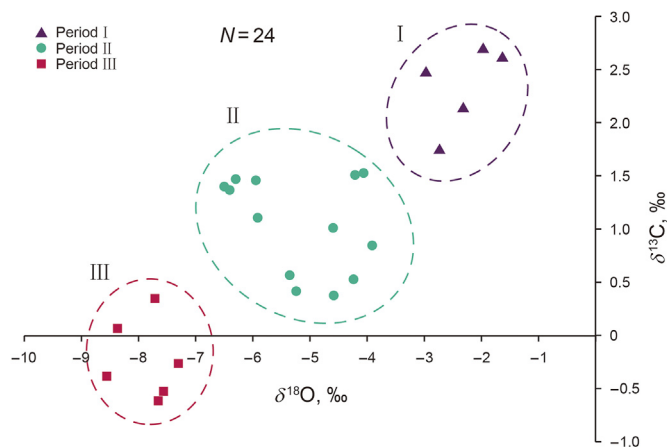


Fig. 8. Characteristics of $\delta^{13}\text{C}$ and $\delta^{18}\text{O}$ isotopes of fracture fills.

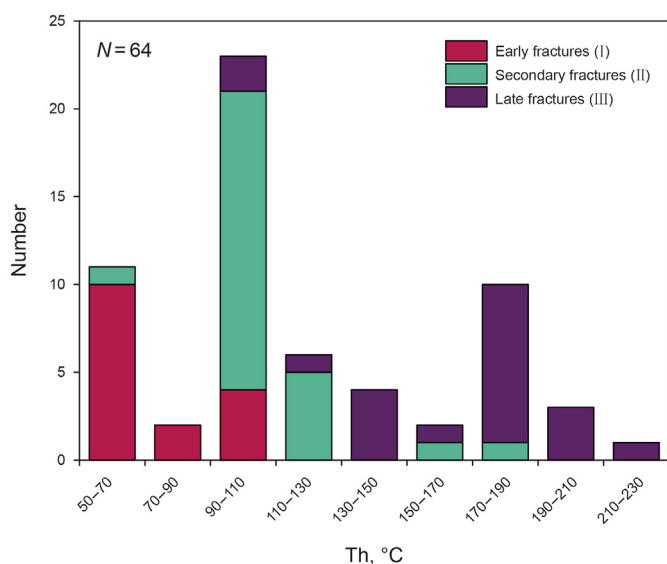


Fig. 9. Frequency distributions of homogenization temperatures (Th).

fractures exhibit historical inheritance evolution. On the other hand, the paleo-temperature is expressed by the equation (Fritz and Smith, 1970):

$$T = 31.9 - 5.55(\delta^{18}\text{O} - \delta^{18}\text{O}_w) + 0.7(\delta^{18}\text{O} - \delta^{18}\text{O}_w)^2$$

where T is the paleo-temperature at which filled calcite formed. $\delta^{18}\text{O}_w$ refers to the oxygen isotope value of the aqueous medium, which is 2‰ according to the previous study (Huang et al., 2011).

The $\delta^{13}\text{C}$ and $\delta^{18}\text{O}$ distributions can be clearly divided into three stages. During the first period, the $\delta^{13}\text{C}$ ranges from 1.7‰ to 2.7‰ and $\delta^{18}\text{O}$ between -3.0 ‰ and -1.6 ‰, with average of -0.2 ‰ and -7.9 ‰, respectively. The average surface temperature is 20 °C and the geothermal gradient is 2.5 °C/100 m in the study area. The calculated formation temperatures ranged between 61.3 and 76.8 °C, indicating that these fracture fills formed at an average burial depth of 1650–2270 m during the Middle Triassic. The Leikoupo Formation was slightly uplifted and experienced denudation in the time of 240–250 Ma.

The $\delta^{13}\text{C}$ and $\delta^{18}\text{O}$ of calcite fills in second stage fractures vary from 0.4‰ to 1.5‰, and from -6.5 ‰ to -3.9 ‰, averaging 1.1‰

and -5.2 ‰, respectively. Calculated formation temperature of these fillings are between 89.2 °C and 129.7 °C. These fractures fillings were formed at burial depth from 2770 to 4380 m during the Late Triassic and the Early Jurassic, which is corresponding to the middle-late Indosinian tectonic movement in 200–220 Ma (Fig. 12).

The $\delta^{13}\text{C}$ ranges from -0.6 ‰ to 0.4‰, and $\delta^{18}\text{O}$ is between -8.6 ‰ and -7.3 ‰, with an average of 2.4‰, and -2.3 ‰, respectively. The paleo-temperature of these fillings were between 144.1 °C and 168.4 °C, with corresponding burial depth ranges from 4960 to 5940 m in the Early Cretaceous. This result indicates the middle Yanshanian tectonic movement in 130–140 Ma.

In these multiperiod fractures, one set is the early weathering fractures presenting an amorphous network structure, which is filled by calcite (Fig. 5d and e). For the structural fractures of the second period, there are mainly high-angle or vertical fractures that are filled by carbonate, in which the fracture planes are relatively smooth (Fig. 5a–c). For the third period of structural fractures, the fractures are fully or partly filled. In addition, the cores show fragmented shapes when they experience substantial deformation or are related to faults (Fig. 5f and g). For the fourth period of structural fractures, most are open without mineral fills and could thus be effective for fluid transport (Fig. 5h–k).

To precisely determine the genesis periods of fractures, the homogenization temperatures (Th) of fracture fillings are projected on the stratigraphic burial history of well TS1 (Fig. 12). The results show that the Th (°C) are vigorously consistent with the paleo-temperature range of burial history in well TS1 and that calculated by the C–O stable isotope. At 240–250 Ma, the first peak in the homogenization temperatures ranging from 50 to 70 °C (Fig. 9) reveals that weathering fractures formed in this period, which occurred during the early Indosinian tectonic movement. At 200–220 Ma, it corresponds to the time of the middle-late Indosinian tectonic movement. The second peak in homogenization temperatures is within the range of 90–110 °C, which implies that the first group of tectonic fractures were developed in this period. At 130–140 Ma, during the middle Yanshanian tectonic movement, the third peak in homogenization temperature ranges from 170 to 190 °C, which demonstrates that the second group of tectonic fractures were developed during this period. Consequently, there are at least three fracture periods (two periods of structural fractures). Additionally, taking the period of unfilled fractures into account, at least three periods stages of structural fractures are certified.

The Pengzhou gas field is located in the western Sichuan Depression, and its tectonic structure is controlled by three major dynamic systems: a) the pushing force of the Yangtze plate from the southeast to the northwest; b) the pushing force of the Qinling orogenic belt from the north to the south; and c) the pushing force of the Tibetan Plateau from the west to the east (Li et al., 2011). The western Sichuan Depression has experienced three tectonic dynamics intervals since the Indosinian period, resulting in a pattern of complex multistage tectonic superposition. As shown in Fig. 13, four major periods of tectonic movement are evident in the Pengzhou gas field area. First, N–S trending compression occurred during the early Indosinian period, resulting in uplift of this area; the Leikoupo Formation experienced weathering, and weathering fractures developed. The dense and uniform weathering fracture fillings were the earliest formed and highly filled by the argillaceous.

Subsequently, during the late Indosinian period, the Pengzhou area was under the maximum principal stress oriented in the NW–SE direction, which produced the conjugate shear fractures trending NNW ($345^\circ \pm 5^\circ$) and W–E ($275^\circ \pm 5^\circ$) (Fig. 13e). The “X” plane conjugated shear fractures were developed before it obvious

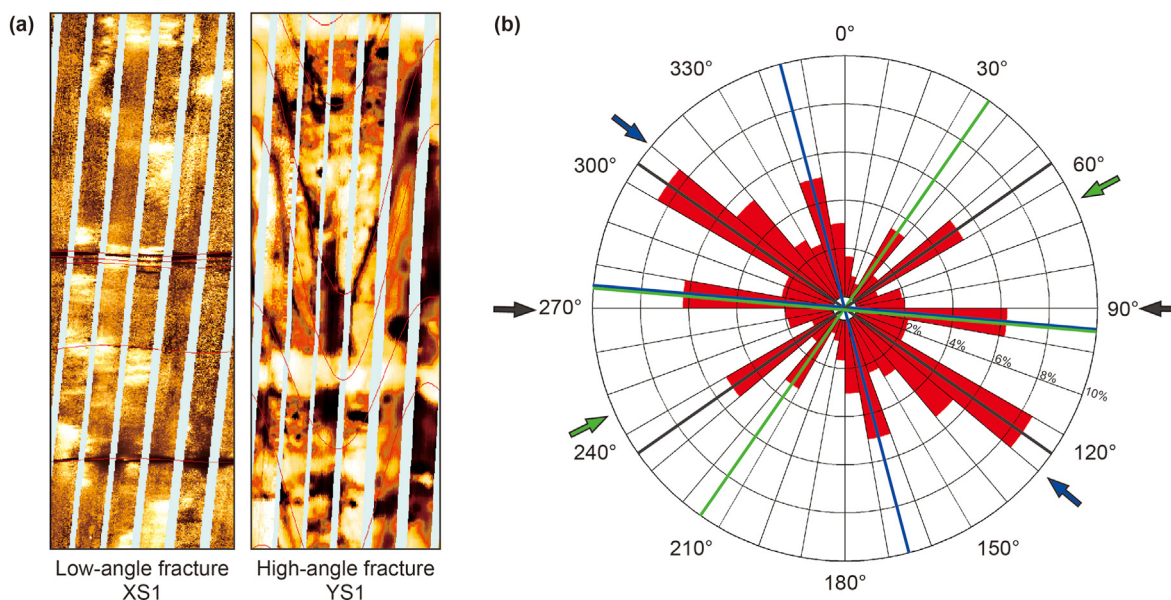


Fig. 10. (a) Partial FMI logging images and (b) rose diagram of the strikes of fractures.

deformation. The fracture fillings were the earliest formed and highly filled by the secondary calcite. They extended under NW-SE tectonic compression and eventually formed the NNW and NWW fault systems.

During the middle Yanshanian tectonic movement, it was subjected to the N–S horizontal compression from the thrust nappe belt of Micang and Daba mountain. A group of “X” plane conjugate shear fractures trending NE ($35^\circ \pm 5^\circ$) and W-E ($275^\circ \pm 5^\circ$) (Fig. 13e) were developed in the Leikoupo Formation.

The fourth tectonic period occurred during the early Himalayan movement, it was continuously subjected to the strong E-W tectonic stress from the arc tectonic zone of Daba mountain. Fold deformation partially occurred in the Leikoupo Formation. Another group of “X” profile shearing fractures that were perpendicular to the principal stress that were developed in NE ($55^\circ \pm 5^\circ$) and SE ($125^\circ \pm 5^\circ$) (Fig. 13e). The tectonic stress field reconstructed and superimposed on the E-W fault systems at the same time, eventually forming the complex fault system in this area.

5.3. Genetic mechanisms of multiperiod fractures

Pinpointing the evolution mechanisms of the Leikoupo Formation in western Sichuan Basin is difficult because of the intricacy of the Longmenshan fault zone. Based on the comprehensive investigations mentioned above, we combined the burial history and tectonic movement periods to analyze the genetic mechanisms of the multiperiod fractures.

By incorporating the characteristics of natural fractures and the tectonic evolution, the mechanism model of the fracture genesis mechanism for natural fractures was constructed. (Fig. 14). The Leikoupo Formation experienced four major episodes of activity that generated various fractures. In the first period, during the late Middle Triassic, the Sichuan Basin was tectonically uplifted under the influence of the early Indosinian movement. The Leikoupo Formation was exposed above the sea surface and was subjected to weathering, denudation, and leaching. The weathering fracture system that developed in the Leikoupo Formation provided channels for the infiltration of surface atmospheric fresh water, resulting in various weathering-related fractures, pores, and caves. Those fractures were mostly filled with calcite, argillaceous material, and gypsum that led to a poor connectivity. In the second period,

around the late Indosinian stage, the Longmenshan orogenic belt was formed by compression of the Sichuan Basin due to the closure of the paleo-Tethys ocean (Zhai, 1989). The area formed wide and gentle anticlines, creating structural fractures, including shear fractures and tensile fractures, which were mostly filled with calcite during the subsequent diagenetic evolution. The fractures of this period are frequently found to be cut by unfilled fractures generated during the later periods or overlapping with them. In the third period, during the middle Yanshanian, the Songpan-Ganzi folded belt and the Longmenshan tectonic belt were thrust to the southeast, transforming the western Sichuan foreland basin into an intracontinental shallow depression basin (Wang et al., 2001). In the meantime, the Pengxian fault and other faults developed in this area. Under the influence of these faults, the strikes of the high-angle fractures were basically the same as those of the faults (mainly trending NE-SW trending). Some fractures were filled by calcite and other minerals during the diagenetic process, while the rest of the fractures were unfilled. In the fourth period, during the early Himalayan stage, the continuous strong uplift of the Longmenshan fault zone, which led to overthrust, slip, and denudation, formed the uplifted fold belt in the western Sichuan Depression (Guo et al., 1996). Under the influence of tectonic movements, NEE and E-W trending high-angle and low-angle shear fractures formed, which in turn were related to high-angle fractures and restrained the expansion of low-angle fractures. Due to the strong tectonic deformation, this is also a crucial time for the development of unfilled tensile fractures. In summary, most fractures from the early periods of the Leikoupo Formation were filled, while the high-angle fractures and vertical fractures from the later periods were unfilled or partly-filled. The weathering fractures and multiperiod structural fractures interpenetrated each other and produced the complex fracture system within the Leikoupo Formation in the Pengzhou gas field.

5.4. Control of fractures on gas migration and production

Although the Leikoupo Formation contains hydrocarbon source rocks, it cannot meet the abundance standard for commercial hydrocarbon accumulation by itself (Liu et al., 2019b; Sun and Liu, 2017; Wu et al., 2017). Previous studies have investigated the origin of gas and gas components in the Leikoupo Formation (Wu

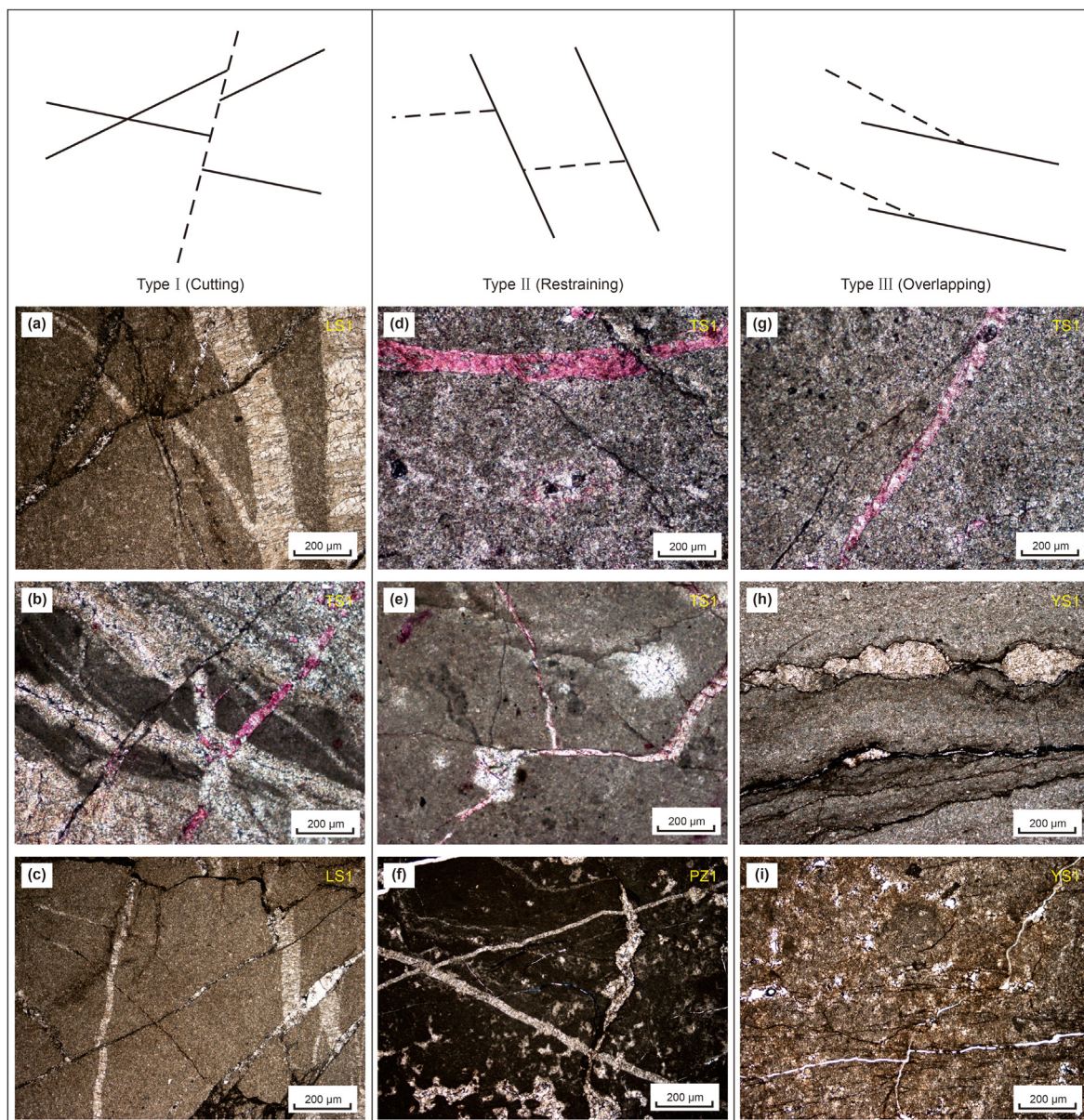


Fig. 11. Three types of fracture interaction relationships. (a)–(i) are crosssectional images of drill cores from the Leikoupo Formation. (a)–(c) from well LS1 and TS1 show that the early stage fractures filled with calcite or other minerals are cut by later unfilled fractures; (d)–(f), from well TS1 and PZ1 present that the early fractures restrain the further extension of the late fractures; (g)–(i) from well TS1 and YS1 show multiple periods filled or unfilled fracture overlapping with each other.

et al., 2020b, 2020c). Geochemical data reveal that bitumen is rare in the Leikoupo Formation, and the most of reservoir natural gas is from oil cracking that did not experience a period of paleo-oil (Dai et al., 1998; Liu et al., 2018, 2019a, 2019b; Wang et al., 1997; Xie, 2015). Five sets of source rocks lie in the marine formations of the Permian strata, which have high hydrocarbon generation potential that provides a strong complement to the Leikoupo gas reservoir (Jin et al., 2018; Liu et al., 2019b; Wu et al., 2020a). The charging paths of hydrocarbons from these source rocks are controlled by faults and fractures (He et al., 2019). The Leikoupo Formation in the western Sichuan Basin experienced the Indosinian movement, Yanshanian movement, and Himalayan movement, resulting in a complex fault and fracture zone that constituted an effective oil and gas migration system. The Permian hydrocarbon source rocks reached the oil-generating window in the middle Indosinian movement. Subsequently, the Permian paleo-oil

reached the cracking period in the late Indosinian or/and early Yanshanian, leading to the generation of a large amount of cracking gas (Chen et al., 2021). The rapid increase in gaseous hydrocarbons results the increase of the formation fluid pressure. The open high-angle and vertical fractures that were generated during later tectonic movements, could provide an effective vertical channel system from source rocks to reservoir formation in the Pengzhou area. Under the influence of high pressure, the gas was rapidly transported to the Leikoupo Formation through the channels formed by the fracture system. A typical reservoir of the Leikoupo Formation, the Lei-4 member gas reservoir, is a fault-related gas reservoir in which faults and fractures bridge multiple source rocks of systems to form a mixed-source gas reservoir. Small fractures may provide channels for fluid transport, while structural microfractures can enhance seepage capacity. Hence, there is a close relationship between fracture development and well production. Based on the

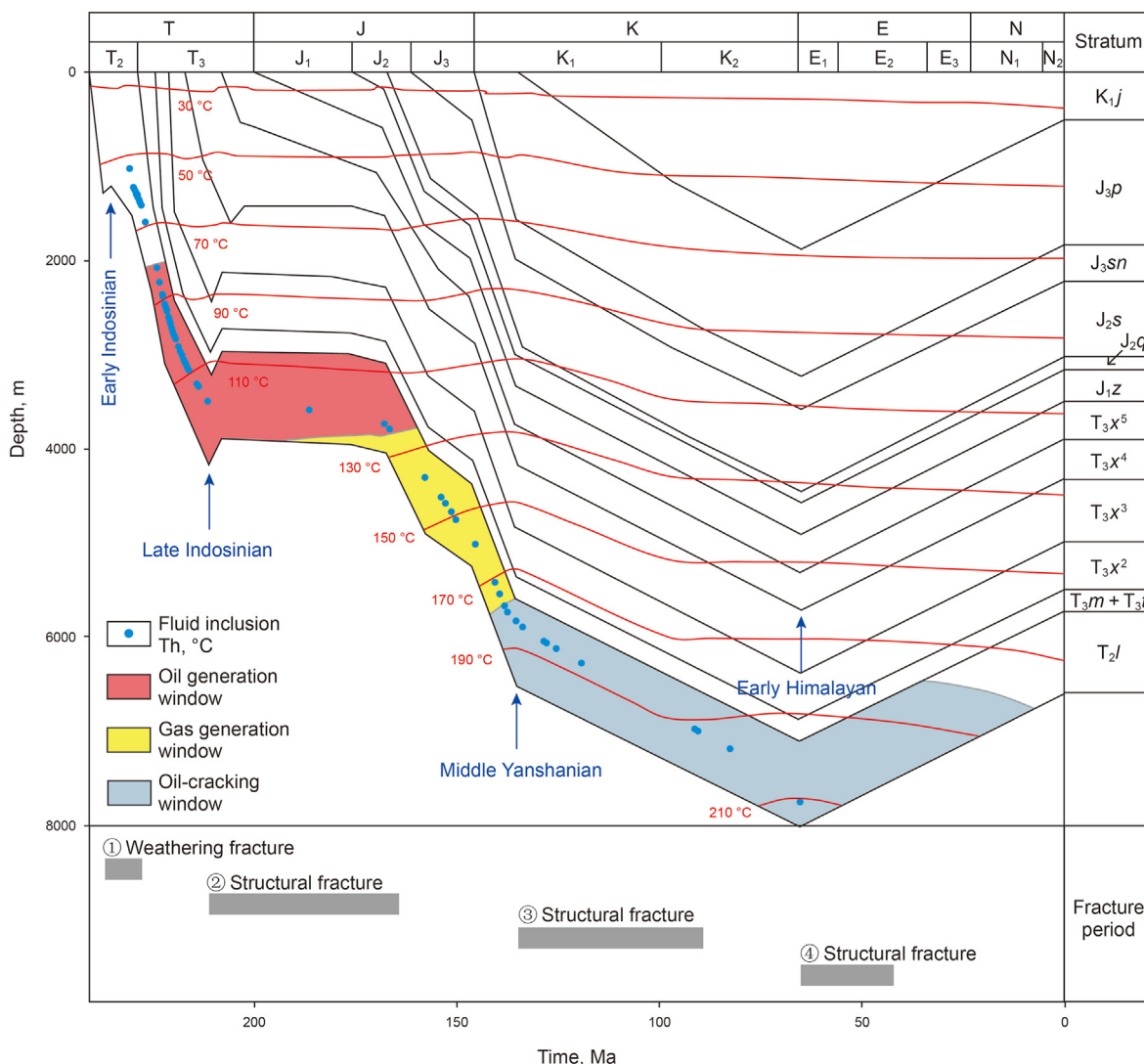


Fig. 12. Burial history of well TS1 in the Leikoupo Formation.

well core investigation, the findings reveal that the linear fracture densities of the seven wells in the Pengzhou gas field are 0.16–3.05/m in the Lei-4 member. Among these wells, the densities of wells YaS1, YS1, and PZ1 are 2.67/m, 2.27/m, and 3.05/m, respectively, as shown in Fig. 15; these three wells have the highest linear fracture densities. At present, the three wells show initial test gas production at very significant amounts of $48.5 \times 10^4 \text{ m}^3/\text{d}$, $60 \times 10^4 \text{ m}^3/\text{d}$, and $115 \times 10^4 \text{ m}^3/\text{d}$, respectively. Therefore, the development degree of the fractures, density and opening degree, closely influences gas productivity. In summary, the third and fourth periods of unfilled structural fractures triggered the oil migration and accumulation of oil-cracking gas in the Leikoupo Formation.

6. Conclusions

Natural fractures in the Middle Triassic Leikoupo Formation in the Pengzhou gas field in the Longmenshan fault belt are mainly structural fractures and weathering fractures. The characteristics of these multiperiod fractures are “X”-shaped conjugate shear structural fractures filled or unfilled to different degrees; the high-angle fractures and vertical fractures are mostly unfilled and usually developed during the multiple tectonic movements in the study area. On the other hand, these multiperiod fractures interacted

with each other and formed three major interaction relationships, including the cutting relationship, restrain relationship, and overlapping relationship.

Complex fractures developed in four major stages related to the four sequential tectonic movements: 1st, weathering fractures that developed during the early Indosinian movement; 2nd, structural fractures related to the late Indosinian movement; 3rd, structural fractures produced by the middle Yanshanian movement; and 4th, structural fractures that formed in the early Himalayan movement.

The unfilled high-angle and vertical fractures that were formed with the later tectonic movements, especially the middle Yanshanian movement and the early Himalayan movement, could provide an effective vertical channel system for migration of hydrocarbons and oil-cracking gas from source rocks to the Leikoupo reservoir in the Pengzhou area. Small fractures may have provided channels for fluid transport, and structural microfractures could enhance seepage capacity. These multiperiod movements formed the comprehensive fractures system in the Middle Triassic Leikoupo Formation in the Pengzhou gas field, which provided potential space for gas migration and accumulation.

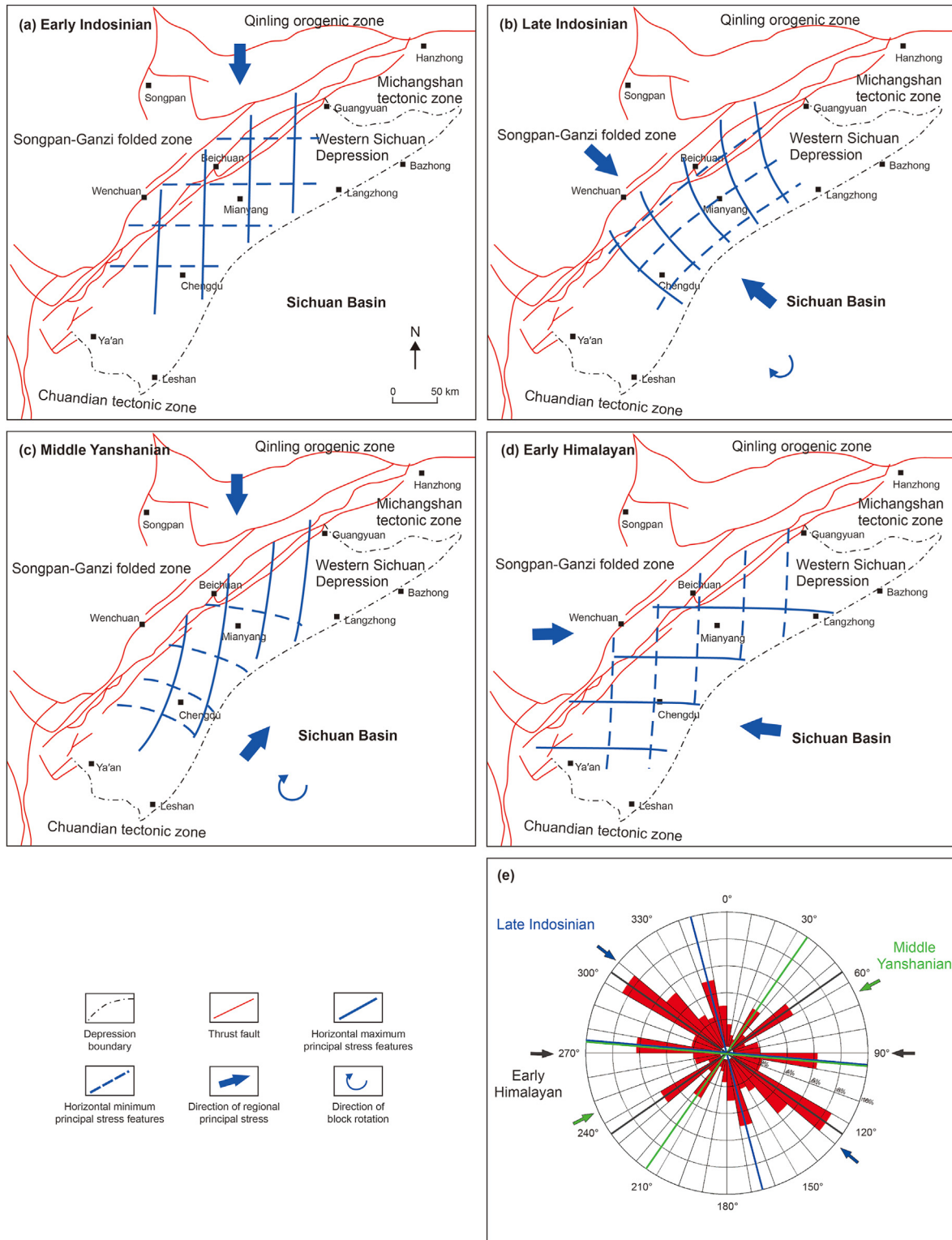


Fig. 13. Schematic diagram of tectonic stress the in the western Sichuan Depression since the Indosinian (modified after Li et al. (2011)). (a) The Early Indosinian period, N-S trending compression; (b) The Late Indosinian period, NW-SE direction stress; (c) The Middle Yanshanian period, NE-SW horizontal compression; (d) The Early Himalayan period, E-W tectonic stress. (e) Rose diagram of the strikes of fractures in the Leikoupo Formation of the Pengzhou area.

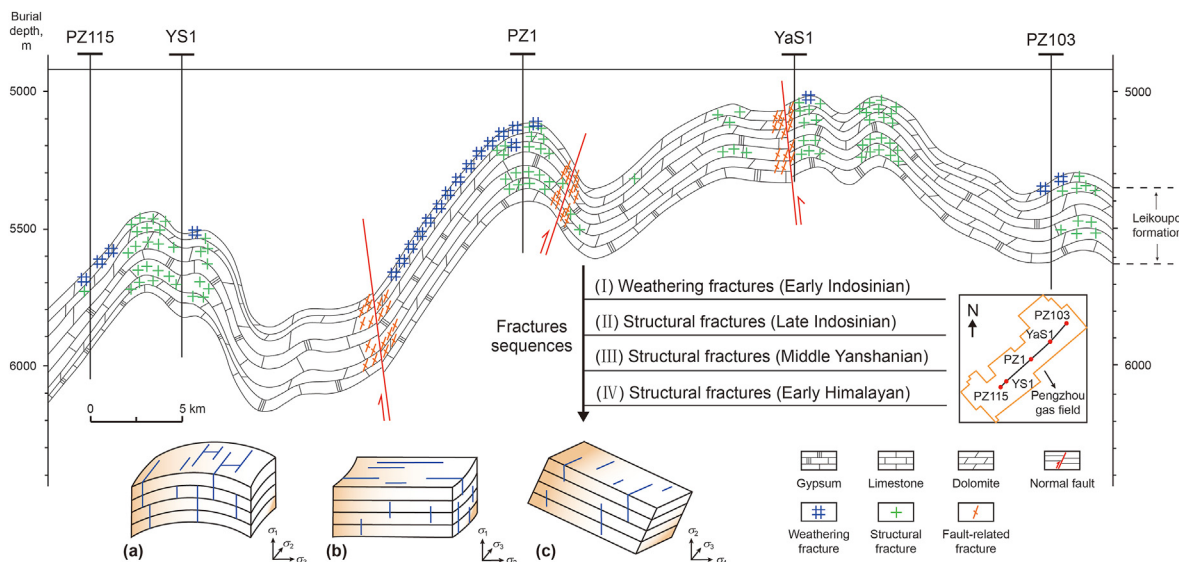


Fig. 14. Fracture evolution pattern of the Leikoupo Formation in the Pengzhou gas field. The distribution of different type of fractures on profile from well PZ115 to PZ103 and the (a), (b), and (c) show the schematic diagram of the formation of tectonic fractures.

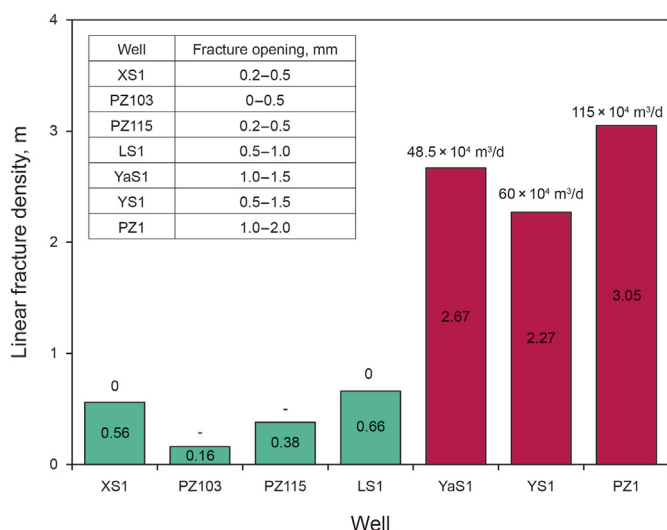


Fig. 15. Comparison of production and fracture characteristics in the Leikoupo Formation. (“-” represents that the well has not been in production or test yield.)

Acknowledgements

The first, second, and fifth authors acknowledge the financial support provided by the National Natural Science Foundation of China (41672133). The second author also acknowledges the National Natural Science Foundation of China (4207021285).

Appendix A. Supplementary data

Supplementary data to this article can be found online at <https://doi.org/10.1016/j.jclepro.2022.133019>.

References

Aghli, G., Moussavi-Harami, R., Mortazavi, S., et al., 2019. Evaluation of new method for estimation of fracture parameters using conventional petrophysical logs and ANFIS in the carbonate heterogeneous reservoirs. *J. Petrol. Sci. Eng.* 172, 1092–1102. <https://doi.org/10.1016/j.petrol.2018.09.017>.

Aghli, G., Moussavi-Harami, R., Tokhmechi, B., 2020. Integration of sonic and resistivity conventional logs for identification of fracture parameters in the carbonate reservoirs (A case study, Carbonate Asmari Formation, Zagros Basin, SW Iran). *J. Petrol. Sci. Eng.* 186, 106728. <https://doi.org/10.1016/j.petrol.2019.106728>.

Ahmadhadi, F., Lacombe, O., Daniel, J.M., 2007. Early Reactivation of Basement Faults in Central Zagros (SW Iran): Evidence from Pre-folding Fracture Populations in Asmari Formation and Lower Tertiary Paleogeography. *Thrust Belts and Foreland Basins*. Springer, pp. 205–228.

Amiri, H., Zare, M., Widory, D., 2015. Nitratennitrogen and oxygen isotope characterization of the Shiraz Aquifer (Iran). *Procedia Earth and Planetary Science* 13, 52–55. <https://doi.org/10.1016/j.proeps.2015.07.012>.

Bakker, R.J., 2003. Package FLUIDS 1. Computer programs for analysis of fluid inclusion data and for modelling bulk fluid properties. *Chem. Geol.* 194 (1–3), 3–23. [https://doi.org/10.1016/S0009-2541\(02\)00268-1](https://doi.org/10.1016/S0009-2541(02)00268-1).

Barker, C.E., Goldstein, R.H., 1990. Fluid-inclusion technique for determining maximum temperature in calcite and its comparison to the vitrinite reflectance geothermometer. *Geology* 18 (10), 1003–1006. [https://doi.org/10.1130/0091-7613\(1990\)018<1003:FITFDM>2.3.CO;2](https://doi.org/10.1130/0091-7613(1990)018<1003:FITFDM>2.3.CO;2).

Bense, V., Gleeson, T., Loveless, S., et al., 2013. Fault zone hydrogeology. *Earth Sci. Rev.* 127, 171–192. <https://doi.org/10.1016/j.earscirev.2013.09.008>.

Bodnar, R.J., 1990. Petroleum migration in the Miocene Monterey Formation, California, USA: constraints from fluid-inclusion studies. *Mineral. Mag.* 54 (375), 295–304. <https://doi.org/10.1180/minmag.1990.054.375.15>.

Bourdet, J., Pironon, J., Levesse, G., et al., 2010. Petroleum accumulation and leakage in a deeply buried carbonate reservoir, Nispero field (Mexico). *Mar. Petrol. Geol.* 27 (1), 126–142. <https://doi.org/10.1016/j.marpetgeo.2009.07.003>.

Branellec, M., Callot, J.P., Nivière, B., et al., 2015. The fracture network, a proxy for mesoscale deformation: constraints on layer parallel shortening history from the Malargüe fold and thrust belt, Argentina. *Tectonics* 34 (4), 623–647. <https://doi.org/10.1002/2014TC003738>.

Burruss, R., Cercone, K., Harris, P., 1983. Fluid inclusion petrography and tectonic-burial history of the Al Ali No. 2 well: evidence for the timing of diagenesis and oil migration, northern Oman Foredeep. *Geology* 11 (10), 567–570. [https://doi.org/10.1130/0091-7613\(1983\)11<567:FIPATH>2.0.CO;2](https://doi.org/10.1130/0091-7613(1983)11<567:FIPATH>2.0.CO;2).

Caine, J.S., Evans, J.P., Forster, C.B., 1996. Fault zone architecture and permeability structure. *Geology* 24 (11), 1025–1028. [https://doi.org/10.1130/0091-7613\(1996\)024<1025:FZAAPS>2.3.CO;2](https://doi.org/10.1130/0091-7613(1996)024<1025:FZAAPS>2.3.CO;2).

Chen, L., Jiang, Z., Liu, K., et al., 2017. Application of Langmuir and Dubinin–Radushkevich models to estimate methane sorption capacity on two shale samples from the Upper Triassic Chang 7 Member in the southeastern Ordos Basin, China. *Energy Explor. Exploit.* 35 (1), 122–144. <https://doi.org/10.1177/0144598716684309>.

Chen, Y., Wu, X., Yang, J., et al., 2021. Research on gas accumulation process in the 3rd sub-member of the 4th member of the middle triassic Leikoupo formation in the western sichuan gas field. *Nat. Gas Geosci.* 32 (11), 1656–1663. <https://doi.org/10.11764/j.issn.1672-1926.2021.07.006>.

CNEA, 2019. Analysis Method for Carbon and Oxygen Isotope of Organic Matter and Carbonate, SY/T 5238-2019. National Energy Institution (in Chinese).

Corfield, R.M., 1995. An introduction to the techniques, limitations and landmarks of carbonate oxygen isotope palaeothermometry. Geological Society, London, Special Publications 83 (1), 27–42. <https://doi.org/10.1144/GSL.SP.1995.083.01.03>.

- Croix, A.D.L., Honari, V., Gonzalez, S., et al., 2018. Impact of sequence stratigraphy on static and dynamic reservoir models: examples from the Precipice–Evergreen succession, Surat Basin, Queensland, 2018 ASEG Extended Abstracts (1), 1–4. https://doi.org/10.1071/ASEG2018abM1_3C.
- Croix, A.D.L., Wang, J., He, J., et al., 2019. Widespread nearshore and shallow marine deposition within the lower jurassic precipice sandstone and evergreen formation in the surat basin, Australia. *Mar. Petrol. Geol.* 109, 760–790. <https://doi.org/10.1016/j.marpetgeo.2019.06.048>.
- Dai, H., Huang, Q., Wang, H., 1998. Study on Natural Gas Lateral Transport: a case study of Moxi gas field in Sichuan Basin. *Nat. Gas Geosci.* 9 (2), 7–11. <https://doi.org/10.11764/j.issn.1672-1926.1998.02.7>.
- Deng, H., Liu, Y., Peng, X., et al., 2018. A new index used to characterize the near-wellbore fracture network in naturally fractured gas reservoirs. *J. Nat. Gas Sci. Eng.* 55, 52–63. <https://doi.org/10.1016/j.jngse.2018.04.018>.
- Ding, X., Wang, B., Wang, X., et al., 2018. The three different types of paleokarstification and reservoir distribution of Leikoupo Formation, Middle Triassic in the northern Sichuan Basin, China. *Carbonates Evaporites* 33 (2), 243–254. <https://doi.org/10.1007/s13146-017-0335-8>.
- Dong, H., Jian, Z., Guang, Y., et al., 2011. The discussion of stratum division and stratum for the Leikoupo formation of middle Triassic in Sichuan basin. *J. Southwest Pet. Univ. Sci. Technol. Ed.* 33 (3), 89–95 (in Chinese).
- Faure, G., 1977. Principles of Isotope Geology.
- Feng, Z., Bao, Z., Wu, S., et al., 1997. Lithofacies palaeogeography of the early and middle triassic of south China. *ScientiaGeologica Sinica* 32 (2), 212–220 (in Chinese).
- Fischer, M.P., Christensen, R.D., 2004. Insights into the growth of basement uplifts deduced from a study of fracture systems in the San Rafael monocline, east central Utah. *Tectonics* 23 (1). <https://doi.org/10.1029/2002TC001470>.
- Freund, S., Beier, C., Krumm, S., et al., 2013. Oxygen isotope evidence for the formation of andesitic–dacitic magmas from the fast-spreading Pacific–Antarctic Rise by assimilation–fractional crystallisation. *Chem. Geol.* 347, 271–283. <https://doi.org/10.1016/j.chemgeo.2013.04.013>.
- Frezzotti, M.L., Tecce, F., Casagli, A., 2012. Raman spectroscopy for fluid inclusion analysis. *J. Geochem. Explor.* 112, 1–20. <https://doi.org/10.1016/j.jexplo.2011.09.009>.
- Fritz, P., Smith, D.G.W., 1970. The isotopic composition of secondary dolomites. *Geochem. Cosmochim. Acta* 34 (11), 1161–1173. [https://doi.org/10.1016/0016-7037\(70\)90056-6](https://doi.org/10.1016/0016-7037(70)90056-6).
- Gao, H., Deng, M., Li, Y., et al., 2018. Diagenesis and reservoir characteristics in the middle Triassic Lei-4 member of Leikoupo formation in Pengzhou area of western Sichuan Basin. *Marine Oil & Gas Geology* 23 (1), 37–46. <https://doi.org/10.3969/j.issn.1672-9854.2018.01.005>.
- Gonzalez, L.A., Lohmann, K.C., 1985. Carbon and oxygen isotopic composition of Holocene reefal carbonates. *Geology* 13 (11), 811–814. [https://doi.org/10.1130/0091-7613\(1985\)13<811:CAOICO>2.0.CO;2](https://doi.org/10.1130/0091-7613(1985)13<811:CAOICO>2.0.CO;2).
- Guo, J., Ren, J., Chen, C., et al., 2019. Comprehensive study of fracture flow characteristic and feasibility of hybrid volume stimulation technique in tight fractured carbonate gas reservoir. *J. Petrol. Sci. Eng.* 174, 362–373. <https://doi.org/10.1016/j.petrol.2018.11.006>.
- Guo, Z., Deng, K., Han, Y., 1996. Formation and Evolution of Sichuan Basin. Geological Publishing House, Beijing, China, p. 200 (in Chinese).
- Hardy, H.R., 1972. Application of Acoustic Emission Techniques to Rock Mechanics Research. Acoustic Emission. ASTM International.
- Hardy, H.R., 1981. Applications of Acoustic Emission Techniques to Rock and Rock Structures: a State-Of-The-Art Review, Acoustic Emissions in Geotechnical Engineering Practice. ASTM International.
- He, D., Ma, Y., Li, Y., et al., 2019. New directions in an established gas play: promising dolomite reservoirs in the middle triassic Leikoupo formation of the Sichuan Basin, China. *AAPG (Am. Assoc. Pet. Geol.) Bull.* 103 (1), 1–29. <https://doi.org/10.1306/05111816502>.
- Homberg, C., Bergerat, F., Angelier, J., et al., 2010. Fault interaction and stresses along broad oceanic transform zone: tjörnes Fracture Zone, north Iceland. *Tectonics* 29 (1). <https://doi.org/10.1029/2008TC002415>.
- Huang, D., Liu, Q., Yang, Y., et al., 2011. Geochemical characteristics of oil seepage and studies of oil source in Maokou Formation, Lower Permian, northwestern Sichuan. *Petroleum Geology & Experiment* 33 (6), 617–623 (in Chinese).
- Hu, X., Su, Y., 2018. Formation mechanism of fractures in the carbonate reservoir of the 4th member of middle triassic leikoupo fm in longmenshan piedmont, Sichuan Basin. *Nat. Gas. Ind.* 38 (11), 15–25. <https://doi.org/10.3787/j.issn.1000-0976.2018.11.002>.
- Huang, W., Cui, Y., Xu, F., et al., 2020. An innovative approach to permeability estimation of the fractured-vuggy carbonate reservoirs based on 2D images. *J. Petrol. Sci. Eng.*, 108293 <https://doi.org/10.1016/j.petrol.2020.108293>.
- Jiang, L., Xu, Z., Shi, S., et al., 2019. Multiphase dolomitization of a microbialite-dominated gas reservoir, the middle triassic Leikoupo formation, Sichuan Basin, China. *J. Petrol. Sci. Eng.* 180, 820–834. <https://doi.org/10.1016/j.petrol.2019.05.014>.
- Jin, Z., Cai, X., Liu, J., et al., 2018. The recent exploration progress and resource development strategy of China Petroleum and Chemical Corporation. *China Petroleum Exploration* 23 (1), 14–25. <https://doi.org/10.3969/j.issn.1672-7703.2018.01.002>.
- Keith, M., Weber, J., 1964. Carbon and oxygen isotopic composition of selected limestones and fossils. *Geochem. Cosmochim. Acta* 28 (10–11), 1787–1816. [https://doi.org/10.1016/0016-7037\(64\)90022-5](https://doi.org/10.1016/0016-7037(64)90022-5).
- Kelly, J., Parnell, J., Chen, H., 2000. Application of fluid inclusions to studies of fractured sandstone reservoirs. *J. Geochem. Explor.* 69, 705–709. [https://doi.org/10.1016/S0375-6742\(00\)00096-0](https://doi.org/10.1016/S0375-6742(00)00096-0).
- Kosari, E., Kadkhodaie, A., Bahroudi, A., et al., 2017. An integrated approach to study the impact of fractures distribution on the Ilam–Sarvak carbonate reservoirs: a case study from the Strait of Hormuz, the Persian Gulf. *J. Petrol. Sci. Eng.* 152, 104–115. <https://doi.org/10.1016/j.petrol.2017.03.001>.
- Levine, J.R., Samson, I.M., Hesse, R., 1991. Occurrence of fracture-hosted impositone and petroleum fluid inclusions, Quebec City region, Canada. *AAPG Bull.* 75 (1), 139–155. <https://doi.org/10.1306/0C9B2763-1710-11D7-8645000102C1865D>.
- Li, B., Hu, B., Luo, Q., et al., 2018. Tectonic sequence and sedimentary evolution in western Hu'nan. *Marine Oil & Gas Geology* 23 (1), 1–12. <https://doi.org/10.3969/j.issn.1672-9854.2018.01.001>.
- Li, H., Tang, H., Qin, Q., et al., 2019. Characteristics, formation periods and genetic mechanisms of tectonic fractures in the tight gas sandstones reservoir: a case study of Xujiache Formation in YB area, Sichuan Basin, China. *J. Petrol. Sci. Eng.* 178, 723–735. <https://doi.org/10.1016/j.petrol.2019.04.007>.
- Li, H., Wang, Q., Qin, Q., et al., 2021a. Characteristics of natural fractures in an ultradeep marine carbonate gas reservoir and their impact on the reservoir: a case study of the Maokou Formation of the JLS Structure in the Sichuan Basin, China. *Energy Fuels* 35 (16), 13098–13108. <https://doi.org/10.1021/acs.energyfuels.1c0158>.
- Li, J., Li, X., Song, M., et al., 2021b. Investigating microscopic seepage characteristics and fracture effectiveness of tight sandstones: a digital core approach. *Petrol. Sci.* 18 (1), 173–182. <https://doi.org/10.1007/s12182-020-00464-8>.
- Li, L., Tan, X., Ding, X., et al., 2011. Difference in depositional characteristics between intra-platform and marginal-platform shoals in Leikoupo Formation, Sichuan Basin and its impact on reservoirs. *Acta Pet. Sin.* 32 (1), 70. <https://doi.org/10.7623/syxb201101010>.
- Li, L., Tan, X., Zhou, S., et al., 2012. Sequence lithofacies paleogeography of Leikoupo formation, Sichuan Basin. *Journal of Southwest Petroleum University (Science & Technology Edition)* 34 (4), 13–22. <https://doi.org/10.3863/j.issn.1674-5086.2012.04.002>.
- Li, S., Xu, G., Song, X., 2016. Forming conditions of Pengzhou large gas field of Leikoupo Formation in Longmenshan piedmont tectonic belt, western Sichuan Basin. *China Petroleum Exploration* 21 (3), 74. <https://doi.org/10.3969/j.issn.1672-7703.2016.03.007>.
- Li, Y., Yu, Q., Liu, P., et al., 2020. Rate transient analysis for coupling Darcy flow and free flow in bead-string fracture-caved carbonate reservoirs. *J. Petrol. Sci. Eng.* 195, 107809. <https://doi.org/10.1016/j.petrol.2020.107809>.
- Li, Y., Kang, Z., Xue, Z., et al., 2018. Theories and practices of carbonate reservoirs development in China. *Petrol. Explor. Dev.* 45 (4), 712–722. [https://doi.org/10.1016/S1876-3804\(18\)30074-0](https://doi.org/10.1016/S1876-3804(18)30074-0).
- Li, Z., Liu, S., Chen, H., et al., 2011. Structural superimposition and conjunction and its effects on hydrocarbon accumulation in the Western Sichuan Depression. *Petrol. Explor. Dev.* 38 (5), 538–551. [https://doi.org/10.1016/S1876-3804\(11\)60054-2](https://doi.org/10.1016/S1876-3804(11)60054-2).
- Lin, Y., Chen, S., 2008. Discussion on the evaporite generating modes, saltforming mechanism and potassium-hunting prospect of Lower-middle Triassic in Sichuan Basin. *J. Salt Lake Res.* 16 (3), 1–10. CNKI:SUN:DZXE.0.2015-11-006 (in Chinese).
- Liu, Q., Jin, Z., Li, J., et al., 2012. Origin of marine sour natural gas and gas-filling model for the Wolonghe Gas Field, Sichuan Basin, China. *J. Asian Earth Sci.* 58, 24–37. <https://doi.org/10.1016/j.jseaes.2012.07.007>.
- Liu, Q., Jin, Z., Wang, X., et al., 2018. Distinguishing kerogen and oil cracked shale gas using H, C-isotopic fractionation of alkane gases. *Mar. Petrol. Geol.* 91, 350–362. <https://doi.org/10.1016/j.marpetgeo.2018.01.006>.
- Liu, Q., Wu, X., Wang, X., et al., 2019a. Carbon and hydrogen isotopes of methane, ethane, and propane: a review of genetic identification of natural gas. *Earth Sci. Rev.* 190, 247–272. <https://doi.org/10.1016/j.earscirev.2018.11.017>.
- Liu, R., Guo, T., Shao, M., 2011. Sources and genetic types of gas in the middle-shallow strata of the Yuanba area, northeastern Sichuan Basin. *Nat. Gas. Ind.* 31 (6), 34–38. <https://doi.org/10.1007/s12182-011-0123-3>.
- Liu, S., Sun, W., Song, J.M., et al., 2019b. The key geological problems of natural gas exploration in the Middle Triassic Leikoupo Formation in Sichuan Basin. *Nat. Gas Geosci.* 30 (2), 412–418. <https://doi.org/10.11764/j.issn.1672-1926.2018.12.011>.
- Liu, Z.L., Tong, J.N., 2001. The Middle Triassic stratigraphy and sedimentary paleogeography of South China. *Acta Sedimentol. Sin.* 19 (3), 327–332. <https://doi.org/10.3969/j.issn.1000-0550.2001.03.002>.
- Lockner, D., 1993. The role of acoustic emission in the study of rock fracture. *Int. J. Rock Mech. Min. Sci. Geomech. Abstracts* 883–899. Elsevier.
- Lyu, W., Zeng, L., Zhang, B., et al., 2017. Influence of natural fractures on gas accumulation in the Upper Triassic tight gas sandstones in the northwestern Sichuan Basin, China. *Mar. Petrol. Geol.* 83, 60–72. <https://doi.org/10.1016/j.marpetgeo.2017.03.004>.
- Meng, N., Shu, L., Wenping, G., 2015. Prediction of dolomite reservoir distribution on top of triassic Leikoupo formation in Chuanxi depression. *China Petroleum Exploration* 20 (3), 30. <https://doi.org/10.3969/j.issn.1672-7703.2015.03.004>.
- Molnar, P., Anderson, R.S., Anderson, S.P., 2007. Tectonics, fracturing of rock, and erosion. *J. Geophys. Res.: Earth Surf.* 112 (F3). <https://doi.org/10.1029/2005JF000433>.
- Mourgues, R., Bureau, D., Bodet, L., et al., 2012. Formation of conical fractures in sedimentary basins: experiments involving pore fluids and implications for sandstone intrusion mechanisms. *Earth Planet Sci. Lett.* 313, 67–78. <https://doi.org/10.1016/j.epsl.2011.10.029>.

- Özkaya, S.I., 2019. Fracture modeling from borehole image logs and water invasion in carbonate reservoirs with layer-bound fractures and fracture corridors. *J. Petrol. Sci. Eng.* 179, 199–209. <https://doi.org/10.1016/j.petrol.2019.04.052>.
- Pang, Y., Soliman, M.Y., Sheng, J., 2017. Investigating gas-adsorption, stress-dependence, and non-Darcy-flow effects on gas storage and transfer in nanopores by use of simplified local density model. *SPE Reservoir Eval. Eng.* 21 (1), 73–95. <https://doi.org/10.2118/187961-PA>.
- Pironon, J., Bourdet, J., 2008. Petroleum and aqueous inclusions from deeply buried reservoirs: experimental simulations and consequences for overpressure estimates. *Geochem. Cosmochim. Acta* 72 (20), 4916–4928. <https://doi.org/10.1016/j.gca.2008.07.019>.
- Ren, L., Lin, C., 2007. Classification methods for development period of fractures and its application: a case study from budate group of hailaer basin. *Acta Sedimentol. Sin.* 2. [https://doi.org/10.1016/S1001-8042\(07\)60056-6](https://doi.org/10.1016/S1001-8042(07)60056-6).
- Roedder, E., 1984. *Fluid Inclusions*, ume 12. Mineralogical Society of America.
- Roedder, E., 1990. Fluid inclusion analysis—prologue and epilogue. *Geochem. Cosmochim. Acta* 54 (3), 495–507. [https://doi.org/10.1016/0016-7037\(90\)90347-N](https://doi.org/10.1016/0016-7037(90)90347-N).
- Saintot, A., Stephens, M., Viola, G., et al., 2011. Brittle tectonic evolution and paleostress field reconstruction in the southwestern part of the Fennoscandian Shield, Forsmark, Sweden. *Tectonics* 30 (4). <https://doi.org/10.1029/2010TC002781>.
- Scheiber, T., Viola, G., 2018. Complex bedrock fracture patterns: a multipronged approach to resolve their evolution in space and time. *Tectonics* 37 (4), 1030–1062. <https://doi.org/10.1002/2017TC004763>.
- Shi, Z., Ma, L., Luo, X., 2010. Formation and evolution of the Guankou fault in the longmen mountains. *Acta Geol. Sin.* 30 (2), 132–135.
- Sichuan Provincial Bureau of Geology and Mineral Resources, 1991. *Regional Geology in Sichuan*. Geological Publishing House, Beijing, China, p. 782.
- Song, W., Liu, L., Wang, D., et al., 2020. Nanoscale confined multicomponent hydrocarbon thermodynamic phase behavior and multiphase transport ability in nanoporous material. *Chem. Eng. J.* 382, 122974. <https://doi.org/10.1016/j.cej.2019.122974>.
- Song, X., Wang, Q., Long, K., et al., 2013. Characteristics and main controlling factors of middle Triassic Leikoupo paleokarst reservoirs in western Sichuan Basin. *Marine origin: Petrol. Geol.* 18 (2), 8–14.
- Sun, W., Liu, S., 2017. Analysis on the formation conditions of large-scale marine deep and super-deep strata gas fields in the middle-northern segments of western Sichuan superimposed Basin, China. *Acta Petrol. Sin.* 33 (4), 1171–1188. CNKI:SUN:YSXB.0.2017-04-012 (in Chinese).
- Talbot, M., 1990. A review of the palaeohydrological interpretation of carbon and oxygen isotopic ratios in primary lacustrine carbonates. *Chem. Geol. Isot. Geosci.* 80 (4), 261–279. [https://doi.org/10.1016/0168-9622\(90\)90009-2](https://doi.org/10.1016/0168-9622(90)90009-2).
- Tang, Y., 2013. Characterization of the sedimentation of the Leikoupo Formation and the weathering crust reservoirs at the top of the formation in the western Sichuan Basin. *Oil Gas Geol.* 34 (1), 42–47. <https://doi.org/10.11743/ogg20130106>.
- Tobin, R.C., Claxton, B.L., 2000. Multidisciplinary thermal maturity studies using vitrinite reflectance and fluid inclusion microthermometry: a new calibration of old techniques. *AAPG Bull.* 84 (10), 1647–1665. <https://doi.org/10.1007/BF00435311>.
- Veizer, J., Demovic, R., 1974. Strontium as a tool in facies analysis. *J. Sediment. Res.* 44 (1), 93–115. <https://doi.org/10.1306/74D72991-2B21-11D7-8648000102C1865D>.
- Wang, E.Q., Meng, Q.R., Chen, Z.I., 2001. Early Mesozoic left-lateral movement along the Longmen Shan fault belt and its tectonic implications. *Earth Sci. Front.* 8 (2), 375–384 (in Chinese).
- Wang, L., Gou, X., Liu, G., 1997. The organic geochemistry and origin of natural gases in Sichuan Basin. *Acta Sedimentol. Sin.* 15 (2), 49–53 (in Chinese).
- Wang, L., Mou, J., Mo, S., et al., 2020. Modeling matrix acidizing in naturally fractured carbonate reservoirs. *J. Petrol. Sci. Eng.* 186, 106685. <https://doi.org/10.1016/j.petrol.2019.106685>.
- Wang, S., Hongming, D., Tingdong, W., 1998. Gas source and migration of high-mature natural gas in Moxi gas field. *Petroleum Explorationist* 3 (2), 5–8 (in Chinese).
- Weil, A.B., Yonkee, W.A., 2012. Layer-parallel shortening across the Sevier fold-thrust belt and Laramide foreland of Wyoming: spatial and temporal evolution of a complex geodynamic system. *Earth Planet. Sci. Lett.* 357, 405–420. <https://doi.org/10.1016/j.epsl.2012.09.021>.
- Wen, Z., He, D., Fan, C., et al., 2013. Analysis of the multi-detachment structure in Micangshan thrust belt, northern Sichuan Basin. *Xinjing Pet. Geol.* 34 (3), 282–286. CNKI:SUN:XJSD.0.2013-03-012 (in Chinese).
- Wu, X., Chen, Y., Liu, G., et al., 2017. Geochemical characteristics and origin of natural gas reservoirs in the 4th member of the middle triassic Leikoupo formation in the western sichuan depression, Sichuan Basin, China. *Journal of Natural Gas Geoscience* 2 (2), 99–108. <https://doi.org/10.1016/j.jnggs.2017.05.001>.
- Wu, X., Chen, Y., Zhai, C., et al., 2020a. Gas-source correlation of natural gas in the Middle Triassic Leikoupo Formation in the Western Sichuan Depression. *Acta Pet. Sin.* 41 (8), 918. <https://doi.org/10.7623/syxb202008002>.
- Wu, X., Chen, Y., Zhai, C., et al., 2020b. Gas source and exploration direction of the Middle Triassic Leikoupo Formation in the Sichuan Basin, China. *J. Nat. Gas Geosci.* 5 (6), 317–326. <https://doi.org/10.1016/j.jnggs.2020.10.001>.
- Wu, X., Liu, Q., Chen, Y., et al., 2020c. Constraints of molecular and stable isotopic compositions on the origin of natural gas from Middle Triassic reservoirs in the Chuanxi large gas field, Sichuan Basin, SW China. *J. Asian Earth Sci.* 204, 104589. <https://doi.org/10.1016/j.jseae.2020.104589>.
- Xie, G., 2015. Source of gas reservoirs in the fourth member of the middle triassic Leikoupo formation in western sichuan depression. *Petroleum Geology & Experiment* 37 (4), 418–422. <https://doi.org/10.11781/syzydz201504418>.
- Xiong, F., Rother, G., Tomasko, D., et al., 2020. On the pressure and temperature dependence of adsorption densities and other thermodynamic properties in gas shales. *Chem. Eng. J.* 395, 124989. <https://doi.org/10.1016/j.cej.2020.124989>.
- Yang, H., Sun, S., Cai, L., et al., 2011. A new method of formation evaluation for fractured and caved carbonate reservoirs: a case study from the Lundong area, Tarim Basin, China. *Petrol. Sci.* 8 (4), 446–454. <https://doi.org/10.1007/s12182-011-0162-9>.
- Yang, R., Fan, A., Van Loon, A., et al., 2014. Depositional and diagenetic controls on sandstone reservoirs with low porosity and low permeability in the eastern Sulige gas field, China. *Acta Geologica Sinica-English Edition* 88 (5), 1513–1534. <https://doi.org/10.1111/1755-6724.12315>.
- Yue, D., Wu, S., Xiong, L., et al., 2018. Reservoir quality, natural fractures, and gas productivity of upper Triassic Xujiahe tight gas sandstones in western Sichuan Basin, China. *Mar. Petrol. Geol.* 89, 370–386. <https://doi.org/10.1016/j.marpetgeo.2017.10.007>.
- Zhai, G.M., 1989. *Petroleum Geology of China: Sichuan Oil and Field 10*. Petroleum Industry Press, Beijing, China (in Chinese).
- Zhang, C., Zhu, D., Luo, Q., et al., 2017. Major factors controlling fracture development in the Middle Permian Lucaoguo Formation tight oil reservoir, Junggar Basin, NW China. *J. Asian Earth Sci.* 146, 279–295. <https://doi.org/10.1016/j.jseae.2017.04.032>.
- Zhang, H., Zhong, Y., Zhang, J., et al., 2020. Experimental research on deterioration of mechanical properties of carbonate rocks under acidified conditions. *J. Petrol. Sci. Eng.* 185, 106612. <https://doi.org/10.1016/j.petrol.2019.106612>.
- Zhang, J., Yin, S., 2017. Fracture gradient prediction: an overview and an improved method. *Petrol. Sci.* 14 (4), 720–730. <https://doi.org/10.1007/s12182-017-0182-1>.
- Zhang, L., Hu, Y., Li, X., et al., 2021. History and key technological progress of natural gas development in the Sichuan Basin. *Nat. Gas. Ind.* 41 (12), 60–72 (in Chinese).
- Zhang, L., Liao, Z., Long, K., et al., 2022. Fundamental constraints of lithologically-controlled fault networks on gas migration and accumulation for fractured carbonates in the western Sichuan Basin, China. *J. Petrol. Sci. Eng.* 208, 109502. <https://doi.org/10.1016/j.petrol.2021.109502>.
- Zhong, Y., Chen, H., Lin, L., et al., 2011. Paleokarstification and reservoir distribution in the Middle Triassic carbonates of the 4th member of the Leikoupo Formation, northeastern Sichuan basin. *Acta Petrol. Sin.* 27 (8), 2272–2280. CNKI:SUN:YSXB.0.2011-08-006 (in Chinese).
- Zhu, G., Zhang, S., Huang, H., et al., 2011. Gas genetic type and origin of hydrogen sulfide in the Zhongba gas field of the western Sichuan Basin, China. *Appl. Geochem.* 26 (7), 1261–1273. <https://doi.org/10.1016/j.apgeochem.2011.04.016>.